Australian Government
Department of Defence
Defence Science and
Technology Organisation

Radiological Source Localisation

Ajith Gunatilaka [1], ***Branko Ristic*** [2], ***and Ralph Gailis*** [1]

[1] **Human Protection and Performance Division**

[2] **Intelligence, Surveillance and Reconnaissance Division**

Defence Science and Technology Organisation

DSTO–TR–1988

ABSTRACT

The problem of localising a point source of gamma radiation is considered. A simplified analytical approach based on the inverse distance square law as well as several probabilistic approaches are described. The problem is studied using the Cramer-Rao bound (CRB) analysis, which quantifies the accuracy with which it is possible to localise the source and estimate its activity. Simulated and real radiological survey data are used to investigate the performance of the algorithms.

APPROVED FOR PUBLIC RELEASE

Published by

DSTO Defence Science and Technology Organisation
506 Lorimer St,
Fishermans Bend, Victoria 3207, Australia

Telephone: (03) 9626 7000
Facsimile: (03) 9626 7999

© *Commonwealth of Australia 2007*
AR No. 013-892
July, 2007

APPROVED FOR PUBLIC RELEASE

Radiological Source Localisation

Executive Summary

The increasing threat of chemical, biological and radiological (CBR) attacks has resulted in a significant interest in research on countering such attacks. Our research focuses on countering radiological attacks, which may, for example, be carried out using radiological dispersion devices or dirty bombs. The ability to rapidly localise a radiological source can assist emergency responders to disable, isolate or safely remove such a device.

This report describes some preliminary work we have carried out in the area of radiological source modelling and localisation. This work concerned localisation of a single fixed gamma radiation source of unknown activity level. The accuracy with which the source location and the activity could be estimated was studied using the Cramer Rao bound analysis. A simple deterministic analytical approach as well as several probabilistic estimation techniques were investigated using simulated and real measurement data.

The inverse square law-based deterministic solution developed in this work uses radiation measurements collected at four arbitrary points to estimate the source position and activity. This algorithm was able to provide reasonable source estimates based on real data collected using the Low Cost Advanced Airborne Radiological Survey (LCAARS) system developed by DSTO.

The maximum likelihood estimator and a nonlinear least squares estimator yielded quite accurate estimates. While the maximum likelihood is an asymptotically efficient estimator, it is a batch algorithm and is unattractive for operational use. An inexact recursive least squares algorithm was developed and it produced good estimates when applied to real data. Unscented Kalman filter (UKF) and extended Kalman filter (EKF) algorithms were also investigated. The UKF approach performed well but the EKF was divergent and could not return acceptable source estimates.

The preliminary investigations described in this report have provided useful insights to the issues associated with radiological source estimation. Future work will investigate more robust estimation techniques and also consider multiple possibly moving sources, localisation in the presence of obstructions and observer motion optimisation.

Authors

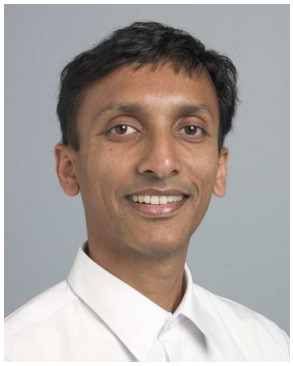

Ajith Gunatilaka
Human Performance and Protection Division

Ajith Gunatilaka obtained his PhD in Electrical Engineering from The Ohio State University, USA in 2000. He obtained a B.Sc. (Engineering) degree with First Class Honours in Electronics and Telecommunication Engineering from The University of Moratuwa, Sri Lanka in 1990. Dr Gunatilaka joined DSTO's HPPD in November 2005 as a defence scientist.

Branko Ristic
Information Surveillance and Reconnaissance Division

Branko Ristic has been involved in R&D projects related to signal processing, estimation, tracking and classification for more than 20 years. Dr. Ristic received all of his degrees in electrical engineering: Ph.D. from QUT 1995, M.Sc. Belgrade University 1991, B. Eng. University of Novi Sad 1984. Since 1996 he has been with DSTO, where his role has been to carry out research, develop new capabilities and provide technical advice to the ADO on the topics of target tracking, sensor fusion, and network enabled surveillance.

Dr Ristic has published over 80 technical papers and presented several invited talks and short courses in Australia, Europe and the US. He is lecturing a post-graduate subject at Adelaide University (subject "Multi-Sensor Data Fusion"). He served on technical committees of several international conferences, and is the Chair of the Fourth Australian Data Fusion Symposium (IDC-07). Dr Ristic won twice the best paper award (at Information Fusion 2005, Philadelphia, USA and DICTA 2005, Cairns, Australia), and recently co-authored a best-selling book: Beyond the Kalman filter: Particle filters for tracking applications (Artech House, 2004).

Ralph Gailis
Human Performance and Protection Division

Ralph Gailis completed his undergraduate studies in physics and mathematics (Honours) at the University of Melbourne in 1992. He went on to do a Ph.D. on the topic of "Plasma Physics in the Early Universe" in the School of Physics, University of Melbourne from 1993–1996. 1997–1998 saw him continue on in the same department as a postdoctoral research fellow, until his recruitment in the Combatant Protection and Nutrition Branch at DSTO in 1999. Research interests at the University of Melbourne included statistical mechanics, general relativity, cosmology and plasma physics.

Since working at DSTO, Ralph has developed a programme on hazard assessment of chemical, biological and radiological weapons. The main focus of scientific research in this area has been in atmospheric dispersion modelling and turbulence theory. This has involved some challenging theoretical work, as well as experimental science in wind tunnel and water channel simulations of dispersion processes. The work has also involved operational support to provide the ADF with current state-of-the-art CBRN hazard prediction models, which have been used for a number of high profile events.

Ralph spent over a year in 2002–2003 working at DRDC (Suffield), Alberta, Canada under a Defence Science Fellowship, greatly extending his knowledge on the science behind CBR hazard assessment and dispersion modelling. He has also served the last six years as National Leader, TTCP CBD Group Technical Panel 9 (Hazard Assessment). These invaluable international interactions have helped the development of the DSTO programme in this area immensely.

Contents

Appendices

Figures

Tables

1 Introduction

Enhancing the chemical, biological and radiological (CBR) situational awareness of the battlefield is an important goal of DSTO research. Accurate assessment and modelling of CBR hazards are essential for the purposes of safely locating and removing or isolating them. Hazard modelling also makes it possible to predict the impact of CBR hazards on surrounding geographical areas and populations. Atmospheric dispersion modelling tools, such as Hazard Prediction and Assessment Capability (HPAC), together with accurate weather data provide a powerful and convenient way to determine how a release of a known CBR source would disperse and what kind of hazardous exposure it would cause in an area. This forward modelling capability provided by HPAC and similar tools is useful in assessing who is vulnerable to the effects of a known CBR source that exists at a known location. It would generally be expected that a CBR source is not known. Sometimes approximate prior knowledge about the CBR source and its location may be available, for example through intelligence information. The exact nature of the source and its location need to be ascertained by using sensor measurements and appropriate source estimation algorithms. A previous DSTO report[1] outlined DSTO's planned work towards CBR source term estimation, hazard modelling and data fusion.

Because CB detection technologies are relatively immature and also because other nations in the TTCP have devoted limited attention to the radiological problem [1], it has been decided to focus DSTO's initial work in this area to radiological source estimation. Another reason for choosing to initially work with the radiological source problem is the availability of the DSTO-developed Low Cost Advanced Radiological Survey (LCAARS) system for data collection to support testing and validation of algorithms. DSTO intends to undertake work in CB hazard modelling and data fusion in future. This report describes our initial work in radiological hazard modelling and source term estimation.

The ultimate goal of radiological source estimation research is to be able to track a dispersing cloud of radioactive particles and predict the integrated radiation dose emitted in all directions from the cloud. Before we can solve this rather complex problem, it is essential to gain a better understanding of the relevant issues by first tackling the relatively simpler problem of estimating a single radiological point source. Once this initial problem is tackled, future research will consider the problem of estimating multiple point gamma sources. The overview of research plan discussed in Section 4.2 of [1] suggests to consider the problem of locating a point gamma radiation source as a first enhancement of LCAARS, and to test these algorithms in a field trial.

2 Description of the problem

Radiation is energy that originates in atomic or nuclear processes and travels through space and materials. Radiation may include fast electrons including beta particles, heavy charged particles such as alpha particles, electromagnetic radiation including X-rays and gamma rays, and neutron radiation [2]. Alpha radiation travels only short distances through air and is unable to penetrate clothing or human skin. Alpha-emitting material may, however, be hazardous if they enter the body through inhalation or other means.

Beta radiation has higher penetration than alpha radiation and may moderately penetrate human skin. Internal deposition of beta-emitting material can be harmful. Devices such as thin-window Geiger-Müller probes can detect the presence of alpha or beta sources. Because of limited distances travelled by alpha and beta radiation, stand-off detection of these sources is difficult. Gamma rays, in contrast, are highly penetrating and may be detected at large distances from the source.

Developing a capability to accurately pinpoint the location of an unknown source of gamma radiation, (eg. a dirty bomb) can help rapid identification and removal of such threats. As mentioned above, currently, radiation survey data collected with the LCAARS system has to be loaded into a mapping software and a two-dimensional intensity plot produced to visually identify the area with the highest intensity as the putative source location. If the source lies outside the surveyed area, then its position cannot be determined using this approach. The gradient of the data may provide an indication of the direction of the source location, which may then be used as a cue for a fresh survey. The goal of the current work is to investigate approaches to improve the accuracy and the efficiency of locating gamma radiation sources, preferably in real time.

Consider a single radiological point source located at (x_0, y_0) in the two-dimensional Cartesian coordinate system (Fig. 1). For simplicity, the elevation of the source is not considered. A radiation survey instrument is used to collect measurements of radiation z_k at Cartesian coordinates (x_k, y_k), where $k = 1, \ldots, N$ and N is the total number of measurements. It is assumed that $\{(x_k, y_k); k = 1, \ldots, N\}$ are known (measured using a GPS receiver for example). The goal is to estimate the location and the strength of the unknown source based on these measurements.

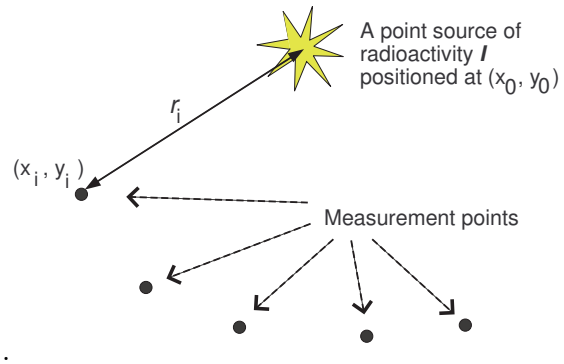

Figure 1: *Geometry of the radiological point source localisation problem*

The dose rate D (measured in units of μSv/h) at a distance r (m) from a point gamma source can be written as[3]:

$$D = \frac{ME}{6r^2} \tag{1}$$

where M is the source activity in MBq and E is the gamma energy per disintegration in MeV.

We can rewrite Equation (1) in the following familiar form of the inverse squared distance law:

$$D = \frac{I}{r^2} \tag{2}$$

where

$$I = \frac{ME}{6}. \tag{3}$$

Here the single parameter I is used to characterise the product of the radioactivity of the source and the gamma energy per disintegration. From Equation (2), I can also be interpreted as the dose rate measured at a distance of 1 m from the source. In some cases the gamma energy E may be known, for example through gamma spectroscopy and, therefore, an estimate of I can be used to compute the source activity M. Therefore, for simplicity, in this report we may refer to I as activity.

When the LCAARS system is used in conjunction with the standard gamma probe, it measures the dose rate and records in units of mSv/h. Therefore the estimated activity will be in GBq.

If the LCAARS system is used with the Micro-R probe, the survey data will be count rates expressed as counts per minute (CPM). In this case, Equation(1) must be modified to incorporate the energy response (CPM/μSv/h) of the probe. Therefore,

$$\text{Count Rate} = \frac{ME}{6r^2} \times \text{Energy Response} \tag{4}$$

$$= \frac{I}{r^2} \tag{5}$$

where

$$I = \frac{ME}{6} \times \text{Energy Response} \tag{6}$$

From Equation (5) we can interpret I as the count rate measured at a distance of 1 m away from the source.

The Micro-R probe has an energy response of 12200 CPM/μSv/h for 0.662 MeV gamma radiation of ^{137}Cs and 6700 CPM/μSv/h for 1.25 MeV average gamma energy of ^{60}Co source [4]. Assuming that the energy of the measured radiation is known, the source radiative activity M can be computed using Equation (6) and the estimated value of I. Therefore, we can represent the unknown point gamma radiation source by defining a parameter vector as follows:

$$\mathbf{x} = \begin{bmatrix} x_0 & y_0 & I \end{bmatrix}^T \tag{7}$$

where T denotes the matrix transpose.

Our goal is to estimate vector $\mathbf{x}$ using measurements $\{z_k; k = 1, \ldots, N\}$ collected at coordinates $\{(x_k, y_k); k = 1, \ldots, N\}$.

3 Deterministic solutions

In simple terms, the point source estimation problem can be considered as estimating the three unknown parameters (x_0, y_0, I). In principle, only three equations in terms of

these three unknowns are necessary to obtain an exact solution. Because the dose rate or the count rate z_k measured at any location (x_k, y_k) depends on the three unknown parameters through the inverse square law, measurements obtained at three different points are all that is required to estimate the source location and strength. Because the solution of these equations involves several square root operations, it produces several spurious solutions in addition to the true estimate, making this solution difficult to use. By including the measurement from a fourth point, these square root operations and, hence, the spurious solutions can be avoided.

Let us consider measurements $\{z_k, k = 1, 2, 3, 4\}$ collected at four arbitrary points (x_k, y_k). If we disregard noise and background radiation, these measurements can be expressed as:

$$z_k(\mathbf{x}) = I/r_k^2, \qquad k = 1, 2, 3, 4 \tag{8}$$

where

$$r_k = \sqrt{(x_k - x_0)^2 + (y_k - y_0)^2} \tag{9}$$

is the distance from the source (x_0, y_0) to the kth measurement point (x_k, y_k).

As shown in Appendix A, Equation (8)can be solved analytically for x_0, y_0 and I, which gives:

$$x_0 = \frac{b_1 c_2 - c_1 b_2}{a_1 b_2 - b_1 a_2} \tag{10}$$

$$y_0 = \frac{a_1 c_2 - c_1 a_2}{b_1 a_2 - a_1 b_2} \qquad \text{and} \tag{11}$$

$$I = z_1 \left[(x_1 - x_0)^2 + (y_1 - y_0)^2\right] \tag{12}$$

where

$$\begin{aligned}
K_1 &= \frac{\left(\frac{1}{z_1} - \frac{1}{z_2}\right)}{\left(\frac{1}{z_1} - \frac{1}{z_3}\right)} \\
K_2 &= \frac{\left(\frac{1}{z_1} - \frac{1}{z_2}\right)}{\left(\frac{1}{z_1} - \frac{1}{z_4}\right)} \\
L_1 &= (x_1^2 - x_2^2) + (y_1^2 - y_2^2) \\
L_2 &= (x_1^2 - x_3^2) + (y_1^2 - y_3^2) \\
L_3 &= (x_1^2 - x_4^2) + (y_1^2 - y_4^2) \\
a_1 &= 2K_1(x_1 - x_3) - 2(x_1 - x_2) \\
b_1 &= 2K_1(y_1 - y_3) - 2(y_1 - y_2) \\
c_1 &= L_1 - K_1 L_2 \\
a_2 &= 2K_2(x_1 - x_4) - 2(x_1 - x_2) \\
b_2 &= 2K_2(y_1 - y_4) - 2(y_1 - y_2) \\
c_2 &= L_1 - K_2 L_3.
\end{aligned}$$

Since the radioactive decay is a stochastic process, the inverse distance square law is applicable to the measurements only in an average sense. Therefore, the count rate or

the dose rate measurements z_k should truly be the averages taken over a sufficiently large number of measurements collected at each measurement point.

The above analytical solution based on four measurements is quite simple and may be useful as a tool to rapidly obtain at least a crude estimate of a radiological point source. There are, however, many limitations in the applicability. The solution assumes a single point source in open space and, therefore, not applicable to multiple source situations or when there are obstacles between the source and the measurement points. For simplicity, the background radiation level was ignored in the derivation discussed above. This is not a major limitation because it is possible in real measurements to subtract the average background from all measurements, provided the background level is relatively constant. The results obtained by applying the four point estimation algorithm to real measurement data is discussed in Subsection 8.2.

4 Statistical data modelling

Accurate statistical modelling of data is essential to the development of effective estimation algorithms. A set of controlled experiments was carried out in June 2006 to collect data to characterise the radiation survey measurements. These experiments were conducted in the radiation laboratory at the DSTO Fishermans Bend site using the low cost advanced airborne radiological survey (LCAARS) system.

The CBRN Defence Centre at DSTO prototyped this survey system using an AN/PDR-77 radiation survey meter equipped with an RS232 interface module, a gamma radiation detector, a GPS receiver, and survey software. Although the system was originally designed for airborne survey, as the name suggests, the DSTO-developed prototype was primarily developed for ground vehicle based survey.

Two different radiation detectors; a standard gamma probe and a Micro-R probe were used. With the standard gamma probe, which is a Geiger-Müller tube, the AN/PDR-77 is capable of measuring gamma radiation over a wide range of dose rates without saturating at high levels but the sensitivity is poor at low dose rates close to background and at low gamma energies. Dose rate data measured with this probe were recorded in milligray per hour (mGy/h). The Micro-R probe uses a 2.54 cm (1 inch) diameter and 3.81 cm (1.5 inch) long NaI scintillation crystal coupled to a 2.54 cm diameter photomultiplier tube operated at 700 volts. It has greater sensitivity to low energy and low dose rate radiation. Measurements with this probe were recorded as count rates in counts per minute (CPM).

Data were collected with each sensor positioned 1 m, 1.5 m, 2 m, 3 m and 4 m away from a 1.647 GBq ^{60}Co radiation source which was enclosed within its transport container to prevent excessive exposure to the experimenter. Background data in the absence of any radiation sources were also collected with each sensor. The data collection software was set up to acquire data for a period of one hour for each different configuration. As the system collects one data point per approximately every two seconds, approximately 1840 measurements were collected in each configuration. The sensors were stationary during data acquisition.

4.1 Dose rate data

The raw dose rate data measured using the gamma probe (in mSv/h) at different distances from the source as well as the data collected in the absence of a source are shown in Figure 2. The variance of these data can be seen to increase with the mean signal level. Figure 3(a) shows the raw data (z_{raw}) collected 3 m away from the radiation source, which show that the measurements fall into a set of discrete levels including 0, 0.00021, 0.00042, 0.00063 mSv/h and other integer multiples of 0.00021. A few measurements are slightly outside these levels having values such as 0.00041 or 0.00062, which may be due to electronic noise in the sensor. All other data sets also displayed similar discreteness. Figure 3(b) shows the normalised data (z_{norm}) that were obtained by applying the transformation:

$$z_{norm} = \text{round}\left(\frac{z_{raw}}{0.00021}\right).$$

Figure 4 shows the normalised histograms of each data set. The mean value μ and the standard deviation σ for each of the data sets are listed in Table 1. From the third and fourth columns of the table we notice that $\sigma \approx \sqrt{\mu}$, as expected for a Poisson distribution. If $z = 0, 1, 2, \ldots$ is the dose rate count, then the Poisson pmf is given by $\mathcal{P}(z;\mu) = e^{-\mu}\mu^z/z!$. Since both the mean and the variance of a Poisson distribution are equal (to μ), for smaller distances between the source and the probe, the probe readings are characterised by higher magnitude but also by higher uncertainty. A Poisson distribution with large μ is approximately Gaussian with mean and variance equal to μ. Observe from Figure 4 that the Gaussian fit is fairly accurate for all cases except for background radiation.

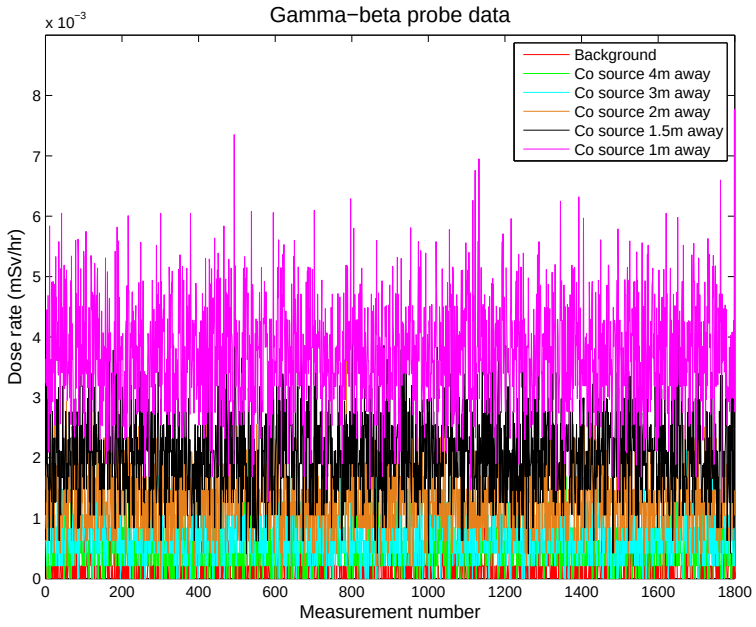

Figure 2: *Raw dose rate data measured with the gamma-beta probe*

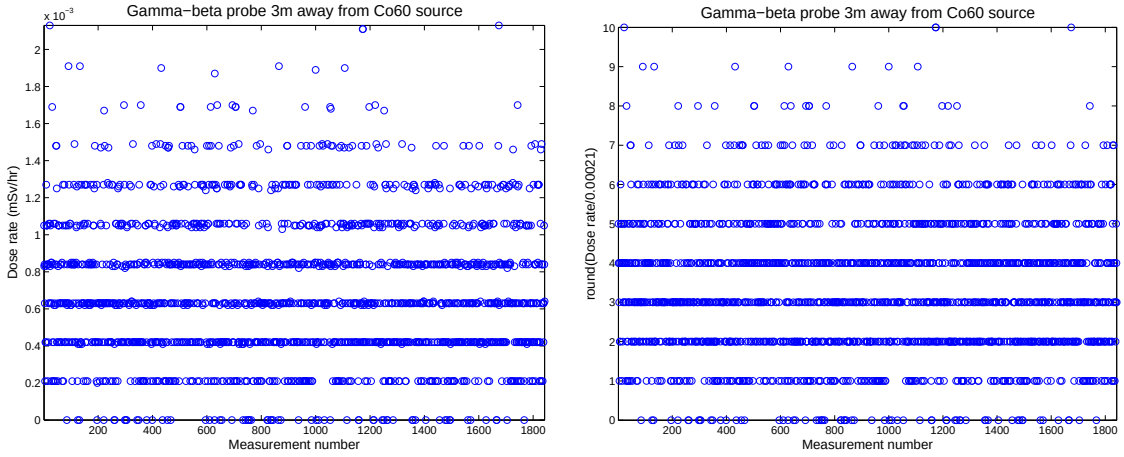

(a) Raw data (b) Normalised data

Figure 3: *Discreteness of dose rate data measured with the gamma-beta probe*

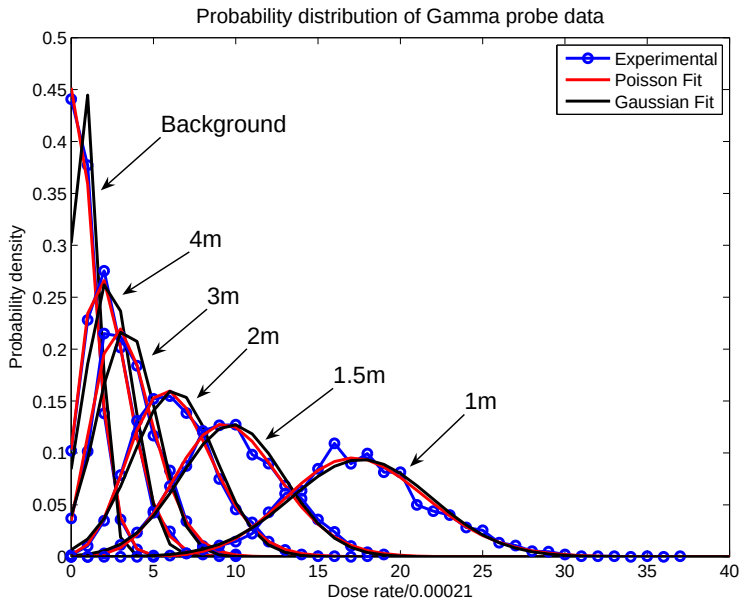

Figure 4: *The histogram for normalised dose rate data and the Poisson and Gaussian distribution fitting.*

If we assume that the mean values of the data measured at different distances from the source to follow the inverse square law, then we can express these mean values as a function of distance as follows:

$$\mu = \frac{I}{d^2} + \mu_0 \tag{13}$$

where μ_0 is the value of μ when the source activity $I = 0$ or the source distance $d = \infty$. Thus μ_0 represents the mean value of the background.

By plotting the measured data and performing a linear fit, we estimate the mean value of the background radiation as $\mu_0 \approx 1.5$. No unit is specified here for μ_0, as we are considering the normalised dose rate, which is dimensionless. Although we assumed the data to follow the inverse square law, and used a linear fit in Figure 5(a) accordingly, from the figure, the data do not seem to follow a straight line fit well.

To check the validity of this assumption let us assume the mean values of the data measured at different distances from the source to obey the following rule:

$$\mu = \frac{I}{d^\alpha} + \mu_0. \tag{14}$$

By taking the logarithm of both sides of Equation (14) we obtain:

$$\log(\mu - \mu_0) = \log I - \alpha \log d. \tag{15}$$

Figure 5(b) shows the plot of Equation (15), where $\mu_0 = 0.7946$ estimated from the background data has been used. The linear fit to the data in Figure 5(b) shows that $\alpha = -1.8$ and $\log I = 2.9$ or $I = \exp(2.9) \approx 18$. Therefore,

$$\mu = \frac{18}{d^{1.8}} + 0.7946. \tag{16}$$

Because $\alpha = -1.8$, rather than -2, this result suggests that the mean values of the measured dose rate data fall off at a rate slightly less than that predicted by the inverse square law. We believe that this less-than-inverse square fall off is due to scattering from the concrete walls of the laboratory. We assume the inverse square law to hold for radiation survey data measured in open space such as in the Holsworthy trial. We intend to verify the validity of this assumption during the next field trial planned for later this year, as the inverse square law was a basic assumption made in developing the estimation algorithms.

Table 1: *The mean value and the standard deviation of dose rate data*

Data set	μ	$\sqrt{\mu}$	σ
1 m	17.6339	4.1993	4.2565
1.5 m	9.7951	3.1313	3.1313
2 m	6.2687	2.5037	2.4900
3 m	3.3643	1.8342	1.8081
4 m	2.2721	1.5074	1.4983
Background	0.7946	0.8914	0.8726

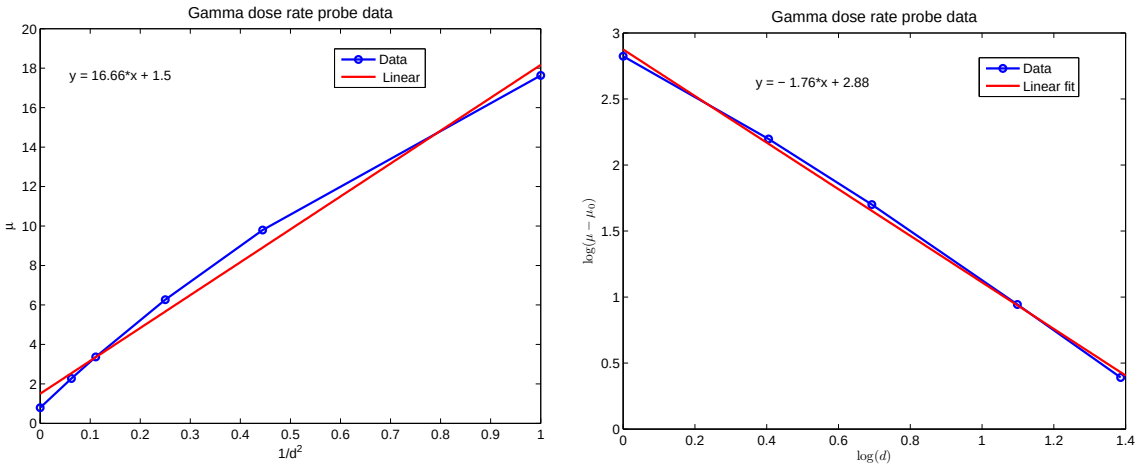

(a) The plot of μ vs. $\frac{1}{d^2}$

(b) The plot of $\log d$ vs. $\log(\mu - \mu_0)$

Figure 5: *Data fitting to dose rate data measured with the gamma-beta probe*

4.2 Count rate data

A plot of the data collected in the laboratory with the Micro-R sensor is shown in Figure 6. The normalised histograms for these data are shown in Figure 7. As in the case of the dose rate data, here also we clearly observe that the uncertainty of data increases with the mean value. A Gaussian function fits these data quite well.

The mean value μ, $\sqrt{\mu}$ and the standard deviation σ for each data set are listed in Table 2. Unlike in the dose rate data, here the variance is not equal to the mean.

Table 2: *Mean value and standard deviation of count rate data*

Data set	μ	$\sqrt{\mu}$	σ
1 m	79151.303	281.338	3693.219
1.5 m	43082.790	207.564	2208.091
2 m	27020.738	164.380	1496.266
3 m	11553.149	107.486	865.810
4 m	6967.930	83.474	651.190
Background	1849.658	43.008	264.925

Let us assume that σ and μ have the following relationship:

$$\sigma = \beta \mu^{\alpha}. \tag{17}$$

Therefore,

$$\log(\sigma) = \alpha \log(\mu) + \log(\beta). \tag{18}$$

By plotting $\log(\sigma)$ versus $\log(\mu)$, as shown in Figure 8(a) and performing a linear fit, we obtain $\alpha = 0.69$ and $\beta = \exp(0.37) = 1.45$. Therefore, we can model the Micro-R

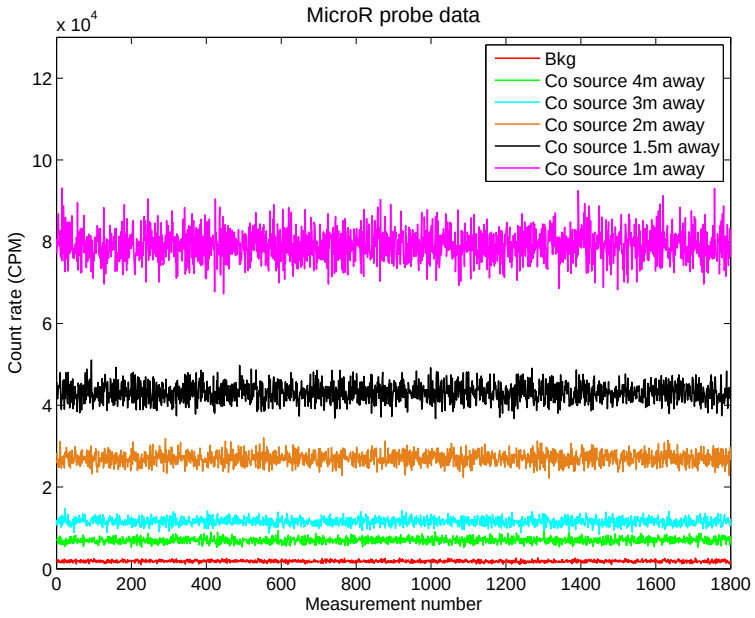

Figure 6: *Raw count rate data collected with the Micro-R probe*

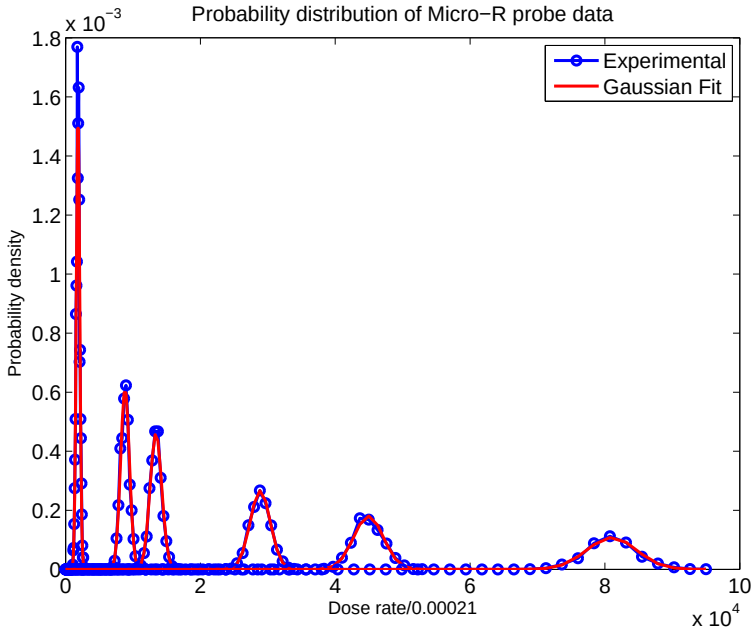

Figure 7: *Normalised histograms and the Gaussian fit for Micro-R probe data*

probe data with a Gaussian distribution whose standard deviation is related to the mean according to the rule:

$$\sigma = 1.45\mu^{0.69}. \tag{19}$$

In Figure 8(b) we plot the relationship between $\log(\mu - \mu_0)$ and $\log(d)$ for count rate data measured with the Micro-R probe at different distances from the source. By using a linear fit to this data we obtain the following model for the mean values of the data as a function of the distance from the source:

$$\mu = \frac{89322}{d^{1.98}} + \mu_0. \tag{20}$$

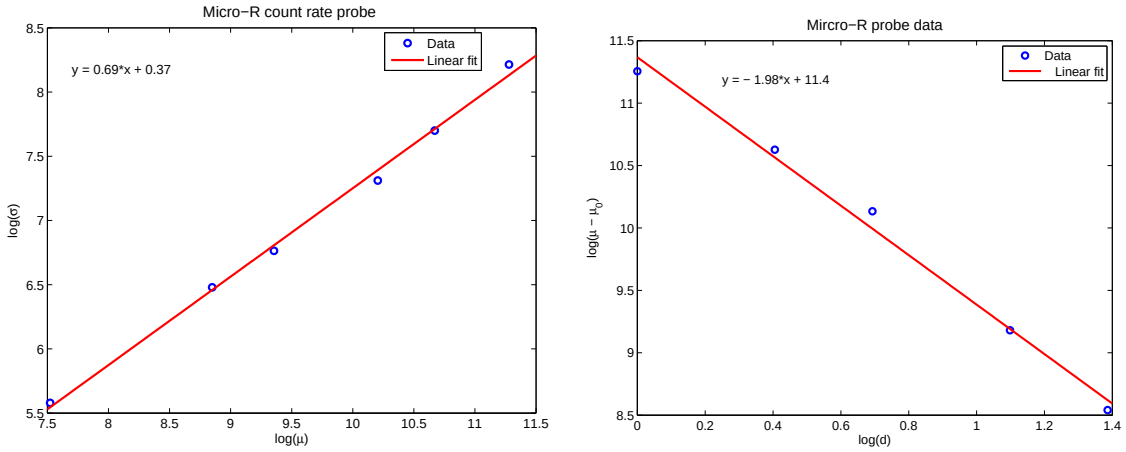

(a) $\log(\mu)$ vs. $\log(\sigma)$ (b) $\log(\mu - \mu_0)$ vs. $\log(d)$

Figure 8: *The characterisation of Micro-R probe data*

5 Probabilistic solutions

Because radioactive decay is an inherently stochastic process, it is reasonable to apply probabilistic techniques for the radiological source estimation problem. Apart from statistical variations in radiation emanating from the source, there is also a randomly fluctuating background radiation level that affects each measurement. The background radiation may comprise contributions due to cosmic radiation, airborne radioactivity, terrestrial radiation, and natural radioactivity of constituent material of the detector itself, other equipment and shielding. The unknown radiation source has to be localised using measurements collected in the presence of this randomly fluctuating background radiation level. This can be considered as a parameter estimation problem where the parameter vector $\begin{bmatrix} x_0 & y_0 & I \end{bmatrix}^T$ has to be estimated based on the set of measurements $\{z_k : k = 1, \ldots, N\}$.

In many parameter estimation problems, the measurements z_k are modelled as a non-linear function of the parameter vector $\mathbf{x}$ with additive noise as follows [5]:

$$z_k = h_k(\mathbf{x}) + v_k. \tag{21}$$

While this model may be appropriate for situations, such as estimating a signal contaminated with noise, it is somewhat different in the problem at hand. In the radiological source estimation problem, the variance in measurements is largely due to statistical fluctuations in the number of disintegrations per unit time in the source itself, rather than due to the measurement noise. Therefore, when the above model is considered for the radiological source estimation problem, $h_k(\mathbf{x})$ may be considered as the mean value of the random parameter vector of interest and v_k the contribution due to its random fluctuations and noise.

In many estimation problems, the measurement noise v_k in Equation (21)can be reasonably modelled using a Gaussian density. A Gaussian noise model is mathematically attractive and usually leads to convenient analytical solutions. Popular nonlinear filtering techniques such as the extended Kalman filter (EKF) and the unscented Kalman filter (UKF) are based on such modelling.

Radiation survey data typically represent samples drawn from a Poisson distribution as was observed in the experimental data collected with the gamma probe. Since the Gaussian extends from $-\infty$ to $+\infty$, it cannot truly represent the radiation survey measurements, which are always non-negative. For large values of measurements, however, a Gaussian with $\sigma = \sqrt{\mu}$ is almost identical to a Poisson distribution with the same mean[1]. The Gaussian assumption will be more applicable for large values of $h_k(\mathbf{x}) = I/r_k^2$, because the truncation point will be far from $\frac{I}{r_k^2}$. By approximating the Poisson distributed measurements by the Gaussian, we are able to model the data reasonably accurately while enjoying the mathematical convenience afforded by the use of the Gaussian distribution.

Hence, for normalised dose rate data, we propose the following model of the measurement likelihood function, given the parameter vector $\mathbf{x}$:

$$p(z_k|\mathbf{x}) = \mathcal{P}\big(z_k; \lambda_k(\mathbf{x})\big) \tag{22}$$

$$\approx \mathcal{N}\big(z_k; \lambda_k(\mathbf{x}), \lambda_k(\mathbf{x})\big) \tag{23}$$

where $\mathcal{N}(z; \mu, \sigma^2)$ denotes a Gaussian density with mean μ and variance σ^2, and

$$\lambda_k(\mathbf{x}) = \frac{I}{(x_k - x_0)^2 + (y_k - y_0)^2} + \lambda_b. \tag{24}$$

Here λ_b represents the mean of the background radiation, that is, the mean of the dose-rate measurements when $I = 0$ or when $d_k = \sqrt{(x_k - x_0)^2 + (y_k - y_0)^2}$ is infinite[2].

In practice the measurements are subjected to a detection threshold. Typically a detection (measurement) is reported only if it exceeds a multiple of the background radiation mean λ_b. Thus the approximation in (23) is valid for all practical purposes. For this case we define an approximate signal-to-noise (SNR) ratio in dB as:

$$\mathrm{SNR}_k[dB] \approx 10 \log \lambda_k \approx 10 \log \frac{I}{d_k^2}. \tag{25}$$

[1]The Micro-R probe data had a different relationship between σ and μ. The reason for this will be investigated

[2]Note that the likelihood function $p(z_k|\mathbf{x})$ was modelled by a truncated Gaussian density in [6].

6 Cramer-Rao analysis

The problem is to estimate the parameter vector $\mathbf{x}$ using the collected measurements $\{z_k : k = 1, \ldots, N\}$ and assuming that the source is localised within a specified region of interest (this information will be our prior knowledge in the Bayesian sense).

6.1 Derivation

In this section we compute the theoretically best achievable second order error performance of any unbiased estimator $\hat{\mathbf{x}}_k$ of the parameter vector. Index k is assigned to the parameter estimate to indicate that k measurements were used in estimation. This estimation error lower bound, known as the Cramér-Rao bound (CRB), will be a good indicator of observability of location and activity of the source.

The CRB, denoted by $\mathbf{C}_k$, provides a lower bound on the mean-square error (MSE) matrix $\mathbf{\Sigma}_k$ of any unbiased estimator $\hat{\mathbf{x}}_k$. The MSE matrix is defined as:

$$\mathbf{\Sigma}_k = \mathbb{E}\left\{ (\hat{\mathbf{x}}_k - \mathbf{x}) (\hat{\mathbf{x}}_k - \mathbf{x})^T \right\}, \tag{26}$$

where $\mathbb{E}$ is the expectation operator. By definition the CRB is given by the inverse of the information matrix $\mathbf{J}_k$, i.e.

$$\mathbf{\Sigma}_k \geq \mathbf{C}_k \equiv \mathbf{J}_k^{-1}. \tag{27}$$

Here the matrix inequality indicates that $\mathbf{\Sigma}_k - \mathbf{C}_k$ is a positive semi-definite matrix. In the Bayesian framework, the information matrix $\mathbf{J}_k$ consists of twofold contribution: prior information and measurement contribution.

Assuming Gaussian model in (23), the information matrix can be computed in the Bayesian framework via the following recursive formula [7, 8]:

$$\mathbf{J}_k = \mathbf{J}_{k-1} + \frac{1}{\lambda_k(\mathbf{x})} \mathbf{H}_k(\mathbf{x})^T \mathbf{H}_k(\mathbf{x}). \tag{28}$$

Here $\mathbf{H}_k(\mathbf{x})$ is the Jacobian of the nonlinear measurement function $\lambda_k(\mathbf{x})$ defined in (24), that is

$$\mathbf{H}_k(\mathbf{x}) = \left[\frac{\partial \lambda_k(\mathbf{x})}{\partial x_0} \quad \frac{\partial \lambda_k(\mathbf{x})}{\partial y_0} \quad \frac{\partial \lambda_k(\mathbf{x})}{\partial I} \right], \tag{29}$$

with individual terms:

$$\frac{\partial \lambda_k(\mathbf{x})}{\partial x_0} = -\frac{2I(x_0 - x_k)}{\left[(x_0 - x_k)^2 + (y_0 - y_k)^2\right]^2} \tag{30}$$

$$\frac{\partial \lambda_k(\mathbf{x})}{\partial y_0} = -\frac{2I(y_0 - y_k)}{\left[(x_0 - x_k)^2 + (y_0 - y_k)^2\right]^2} \tag{31}$$

$$\frac{\partial \lambda_k(\mathbf{x})}{\partial I} = \frac{1}{(x_0 - x_k)^2 + (y_0 - y_k)^2}. \tag{32}$$

The recursion in (28) is initialised with $\mathbf{J}_0$ which corresponds to our prior information (in the Bayesian sense) about the parameter vector. Assuming a Gaussian prior distribution with mean $\hat{\mathbf{x}}_0$ and covariance $\mathbf{P}_0$, we have that $\mathbf{J}_0 = \mathbf{P}_0^{-1}$. The prior mean $\hat{\mathbf{x}}_0$ and covariance $\mathbf{P}_0$ may be obtained, for example, based on intelligence information. If prior information is weak, $\mathbf{P}_0$ will take large values which in the limiting case yields $\mathbf{J}_0 = 0$.

6.2 Analysis

Let us consider first a scenario where the measurements are collected uniformly along a circular path with the source positioned in the centre of the circle. The first measurement is taken at the angle of 45^o from the source with respect to the x-axis, with observer moving anti-clockwise. The activity of the source is fixed at $I = 10^6$, while the radius of the circle takes values of 562.3m, 177.8m and 56.2m, which correspond to SNR values of 5dB, 15dB and 25dB, respectively. The initial covariance is diagonal:

$$\mathbf{P}_0 = \text{diag}\left(\begin{bmatrix}\sigma_x^2 & \sigma_y^2 & \sigma_I^2\end{bmatrix}\right) \tag{33}$$

with $\sigma_x = \sigma_y = 250$m and $\sigma_I = 5 \cdot 10^5$. The choice if these values in our example is arbitrary. The values for σ_x and σ_y are chosen to reflect prior knowledge that the source is located with probability 95% within an elliptical region whose axes are approximately $2\sigma_x$ and $2\sigma_y$. The prior information on source intensity is weak hence σ_I is set to a large value. The best achievable standard deviation of the estimation error in *position*, defined as $\sqrt{C_k[1,1] + C_k[2,2]}$, is plotted in Figure 9(a) for the three values of SNR. Likewise, Figure 9(b) shows the best achievable standard deviation of estimation error in *activity*, $\sqrt{C_k[3,3]}$. Observe how in both figures the error standard deviation reduces as we collect more measurements. The importance of having a high enough SNR is also evident: after processing all 60 measurements, at SNR=15 (versus 5dB) we can achieve the standard deviation of positional estimation error of 5m (versus 50m). CRB analysis allows us to quantify the best achievable estimation accuracy for different values of SNR and for a given scenario.

7 Estimation algorithms and their performance

7.1 Algorithms

In this section we describe several estimation algorithms for estimation of parameter vector $\mathbf{x}$. Parts of this section have been reported in [9].

7.1.1 Maximum likelihood estimation

Since we deal here with parameter estimation, the first algorithm to consider is the maximum likelihood estimator (MLE). The maximum likelihood estimator (MLE) is a block algorithm as it operates on the accumulated set of all previous measurements. It does not use any prior information (hence referred as non-Bayesian) but is widely used for parameter estimation because if an asymptotically unbiased and minimum variance estimator exists for large sample sizes, it is guaranteed to be the MLE [10]. The MLE is determined as the vector $\hat{\mathbf{x}}_N^{ML}$ which maximises the likelihood function $p(z_1, \ldots, z_N|\mathbf{x})$.

$$\hat{\mathbf{x}}_N^{ML} = \arg\max_{\mathbf{x}} \; p(z_1, \ldots, z_N|\mathbf{x}). \tag{34}$$

Assuming that measurements are mutually independent, with the likelihood of each measurement given by Equation (23), the likelihood function becomes:

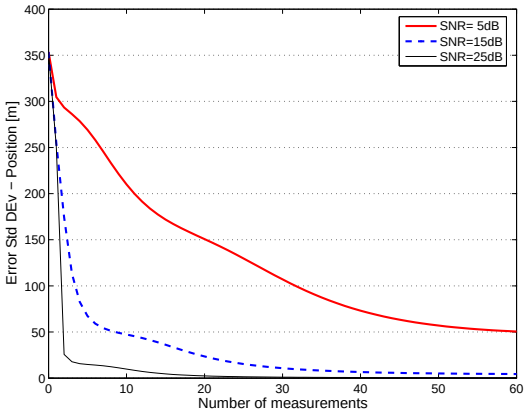

(a)

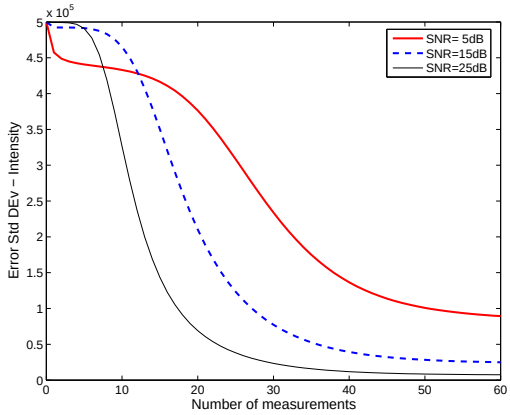

(b)

Figure 9: *CRB analysis: the error standard deviation in (a) position and (b) activity*

$$p(z_1, \ldots, z_N|\mathbf{x}) = \prod_{k=1}^{N} \frac{1}{\sqrt{2\pi\lambda_k(\mathbf{x})}} \exp\left[-\frac{1}{2}\frac{(z_k - \lambda_k(\mathbf{x}))^2}{\lambda_k(\mathbf{x})}\right]. \tag{35}$$

By taking the logarithm of both sides of Equation (35) we obtain:

$$\log p(z_1, \ldots, z_N|\mathbf{x}) = \left(-\frac{1}{2}\right) \sum_{k=1}^{N} \left\{ \log\left(2\pi\lambda_k(\mathbf{x})\right) + \frac{(z_k - \lambda_k(\mathbf{x}))^2}{\lambda_k(\mathbf{x})} \right\}. \tag{36}$$

Then the MLE of Equation (34) becomes:

$$\hat{\mathbf{x}}_N^{ML} = \arg\min_{\mathbf{x}} \left\{ \sum_{k=1}^{N} \frac{(z_k - \lambda_k(\mathbf{x}))^2}{\lambda_k(\mathbf{x})} + \sum_{k=1}^{N} \log(2\pi\lambda_k(\mathbf{x})) \right\}.$$

Minimisation in (34) can be performed by numerical methods [11]; our implementation is based on MATLAB© built-in routine *fminsearch*. Being a non-Bayesian estimator, the MLE is expected to reach the Bayesian CRB (discussed in Section 6) only for large enough sample size (large N) when the influence of prior knowledge has diminished.

7.1.2 Least squares (LS) with reduced search dimension

The least squares (LS) method is another commonly used estimation procedure. If z_k is the kth measurement and $h_k(\mathbf{x})$ its prediction, the LS estimate $\hat{\mathbf{x}}_N^{LS}$ is defined as:

$$\hat{\mathbf{x}}_N^{LS} = \arg\min_{\mathbf{x}} \sum_{k=1}^{N} \left(z_k - h_k(\mathbf{x})\right)^2 . \tag{37}$$

Equation (37) does not make any assumptions about the measurement errors [5]. If these errors are independent and identically distributed zero-mean Gaussian random variables, then the LS estimate coincides with the ML estimate.

Typically, one may directly minimise the sum of squared errors by searching in the three dimensional space spanned by (x_0, y_0, I), for example using the *fminsearch* routine. We consider an alternative approach developed by Takumi et al.[12] in which the search is carried out in only the two dimensional (x_0, y_0) space.

Let f denote the sum of the squared error terms.

$$f(x_0, y_0, I) = \sum_{k=1}^{N} \left(z_k - \frac{I}{r_k^2}\right)^2 \tag{38}$$

where $r_k = \sqrt{(x_k - x_0)^2 + (y_k - y_0)^2}$ is the radial distance from the measurement point to the putative radiation source. At the optimal value of (x_0, y_0, I) that minimises the estimation error f,

$$\frac{\partial f}{\partial I} = 0. \tag{39}$$

From this equation, the optimal value of I can be obtained as a function of (x_0, y_0), i.e.

$$I = \frac{\sum_{k=1}^{N} \frac{z_k}{r_k^2}}{\sum_{k=1}^{N} \frac{1}{r_k^4}}. \tag{40}$$

Equation (40) can be used to compute the value of I at all possible (x_0, y_0) coordinates within an area where the unknown source is assumed to be located. By substituting the computed I in (38), the estimation error is computed at each point. The (x_0, y_0) value pair corresponding to the minimum value of f is chosen as the most likely source location within the search space. Because this approach reduces the search space dimension from 3D to 2D, the minimum can be obtained relatively rapidly. The search may be carried out in more than one stage, where a large area is first searched at a coarse resolution to find the most likely subarea, which will then be searched using a finer resolution search. Instead of simply accepting the minimum solution returned by the algorithm, it may be informative to look at a plot of the squared error surface, which could show other likely source positions. A good example is when data is collected along a linear trajectory. While the algorithm may return the location corresponding to the minimum error, a plot of the error surface may show that an image solution also exists.

Since this is a nonlinear LS estimation problem where according to Equations (23) and (24), additive noise has a non-constant variance, a theoretical prediction of the estimation accuracy would be very difficult to derive.

7.1.3 An approximate recursive LS algorithm

Although the least squares approach is capable of localising the source accurately, being a batch algorithm, it is unattractive for real-time operational use. A batch algorithm requires increasing amounts of memory and processing time as the number of measurements is increased. A recursive algorithm, in contrast, requires essentially the same amount of processing time and memory for each new measurement irrespective of the total number of measurements and is attractive for real-time applications. While a recursive solution is straightforward and widely used in linear least squares problems, it is not the case for non-linear least squares problems. Some possible approaches to derive recursive non-linear least squares solutions are described in the literature [13, 14, 15].

While we intend to investigate these approaches in future and apply them to the radiation source estimation problem, here we describe a simple inexact recursive least squares solution that we developed for initial experimentation. Although it is only an approximate solution, it was able to provide reasonably accurate source estimates when applied to the set of real measurements currently available to us. These results will be presented in Subsection 8.5. To derive this approximate recursive solution, we rewrite Equation (40) as follows:

$$I_N = \frac{\sum_{k=1}^{N} \frac{z_k}{r_k^2}}{\sum_{k=1}^{N} \frac{1}{r_k^4}} = \frac{\mathcal{N}_N}{\mathcal{D}_N} \tag{41}$$

where I_N is the I estimate after observing the Nth observation, z_N, and $\mathcal{N}_N$ and $\mathcal{D}_N$ are the numerator and the denominator of Equation (41). Therefore, the estimate of I after the $(N+1)$th observation can be expressed as:

$$I_{N+1} = \frac{\mathcal{N}_{N+1}}{\mathcal{D}_{N+1}} \tag{42}$$

where:

$$\mathcal{N}_{N+1} = \mathcal{N}_N + \frac{z_{N+1}}{R_{N+1}^2} \tag{43}$$

$$\mathcal{D}_{N+1} = \mathcal{D}_N + \frac{1}{R_{N+1}^4}. \tag{44}$$

Unfortunately, Equation (38) cannot be transformed into a recursive form. Therefore, we tried the following recursive form, which, while not exactly equivalent to Equation (38), tries to approximate it to a limited extent:

$$f_{N+1} = f_N + \left(z_{N+1} - \frac{I_{N+1}}{R_{N+1}^2} \right)^2. \tag{45}$$

The source estimates after observing the $(N+1)$th measurement are computed by searching for the minimum of f_{N+1}. Rigourous approaches to recursive nonlinear least squares will be investigated in future work.

7.1.4 EKF and UKF

The radiological source localisation problem can be formulated within the Bayesian filtering framework [8]. Since the parameter vector is fixed, the state dynamic equation is trivial. The measurement equation (Eqn 23) is highly nonlinear and, therefore, we need to consider a nonlinear filtering solution.

The goal of filtering (the sequential Bayesian estimation) is to determine the posterior pdf $p(\mathbf{x}|z_1, \ldots, z_k)$, for $k = 1, 2, \ldots$. Both the extended Kalman filter (EKF) [5] and the unscented Kalman filter (UKF) [16] approximate this posterior pdf by a Gaussian density $\mathcal{N}(\mathbf{x}_{k|k}, \mathbf{P}_{k|k})$. The mean and covariance of this Gaussian pdf are computed recursively: in the case of the EKF via the local linearisation of the measurement function $h_k(\mathbf{x})$; in the case of the UKF via an approximation of the posterior pdf by a set of deterministically chosen sample (or sigma) points.

Both EKF and UKF are based on approximations and hence suboptimal and prone to divergences (as we will see in Sec.7.2). However, the UKF is a more accurate algorithm since it captures the mean and covariance of the underlying posterior pdf exactly up to the second order of nonlinearity. Both EKF and UKF implementations contain a small and equal amount of process noise.

7.1.5 EKF equations

$$\hat{\mathbf{x}}_{k|k-1} = \mathbf{f}_{k-1}(\hat{\mathbf{x}}_{k-1|k-1}) \tag{46}$$

$$\mathbf{P}_{k|k-1} = \mathbf{Q}_{k-1} + \hat{\mathbf{F}}_{k-1}\mathbf{P}_{k-1|k-1}\hat{\mathbf{F}}_{k-1}^T \tag{47}$$

are the state prediction and state prediction covariance based on measurements up to the $(k-1)$th measurement. The notation $k|k-1$ denotes the prediction of the kth estimate after observing up to the $(k-1)$th measurement. The updated estimate after observing the kth measurement is denoted by $k|k$. $\mathbf{Q}_{k-1}$ is the covariance of process noise.

$$\hat{\mathbf{x}}_{k|k} = \hat{\mathbf{x}}_{k|k-1} + \mathbf{K}_k(\mathbf{z}_k - \lambda_k(\hat{\mathbf{x}}_{k|k-1})) \tag{48}$$

$$\mathbf{P}_{k|k} = \mathbf{P}_{k|k-1} - \mathbf{K}_k\mathbf{S}_k\mathbf{K}_k^T \tag{49}$$

are the updated state and state covariance after receiving the kth measurement z_k.

$$\mathbf{S}_k = \hat{\mathbf{H}}_k\mathbf{P}_{k|k-1}\hat{\mathbf{H}}_k^T + \mathbf{R}_k \tag{50}$$

is the innovation covariance, where the innovation is defined as:

$$\nu_{\mathbf{k}} = \mathbf{z_k} - \lambda_{\mathbf{k}}(\hat{\mathbf{x}}_{\mathbf{k}|\mathbf{k-1}}) \tag{51}$$

and

$$\mathbf{K}_k = \mathbf{P}_{k|k-1}\hat{\mathbf{H}}_k^T\mathbf{S}_k^{-1} \tag{52}$$

is the filter gain or the Kalman gain. $\mathbf{R}_k$ is the covariance of measurement noise. $\hat{\mathbf{F}}_{k-1}$ and $\hat{\mathbf{H}}_k$ are the local liberalisations of nonlinear functions $\mathbf{f}_{k-1}(\mathbf{x})$ and $\lambda_k(\mathbf{x})$, respectively[8].

Because we are trying to estimate the position and the strength of a static source, the state transition equation is simply:

$$\mathbf{x}_k = \mathbf{x}_{k-1}. \tag{53}$$

$$\therefore \mathbf{f}_{k-1}(\mathbf{x}_{k-1}) = \mathbf{x}_{k-1}. \tag{54}$$

and

$$\begin{aligned}
\hat{\mathbf{F}}_{k-1} &= \left[\nabla_{\mathbf{x}_{k-1}} \mathbf{f}_{k-1}^T(\mathbf{x}_{k-1})\right]^T |_{\mathbf{x}_{k-1}=\hat{\mathbf{x}}_{k-1|k-1}} && (55)\\
&= \left[\begin{bmatrix} \frac{\partial}{\partial x_0} \\ \frac{\partial}{\partial y_0} \\ \frac{\partial}{\partial I} \end{bmatrix} \begin{bmatrix} x_0 & y_0 & I \end{bmatrix}\right]^T |_{\mathbf{x}_{k-1}=\hat{\mathbf{x}}_{k-1|k-1}} && (56)\\
&= \mathbf{I}. && (57)
\end{aligned}$$

Using the measurement equation (Eqn (24)) in

$$\hat{\mathbf{H}}_k = [\nabla_{\mathbf{x}_k} \lambda_k^T(\mathbf{x}_k)]^T |_{\mathbf{x}_k=\hat{\mathbf{x}}_{k|k-1}} \tag{58}$$

we get:

$$\begin{aligned}
\hat{\mathbf{H}}_k &= \left[\begin{bmatrix} \frac{\partial}{\partial x_0} \\ \frac{\partial}{\partial y_0} \\ \frac{\partial}{\partial I} \end{bmatrix} \left[\frac{I}{(x-x_0)^2+(y-y_0)^2} + \lambda_b\right]\right]^T |_{\mathbf{x}_k=\hat{\mathbf{x}}_{k|k-1}} && (59)\\
&= \left[\frac{2I(x-x_0)}{[(x-x_0)^2+(y-y_0)^2]^2} \quad \frac{2I(y-y_0)}{[(x-x_0)^2+(y-y_0)^2]^2} \quad \frac{1}{(x-x_0)^2+(y-y_0)^2}\right] |_{\mathbf{x}_k=\hat{\mathbf{x}}_{k|k-1}}. && (60)
\end{aligned}$$

7.1.6 UKF equations

In the case of the UKF, the posterior density at time $k-1$ is assumed to be Gaussian and this density is represented by a set of M sample points χ_{k-1}^i and corresponding weights W_{k-1}^i, which can be computed according to the unscented transform [8].

Then the predicted state and the state prediction covariance are given by:

$$\hat{\mathbf{x}}_{k|k-1} = \sum_{i=0}^{M-1} W_{k-1}^i \cdot \mathbf{f}_{k-1}(\chi_{k-1}^i) \tag{61}$$

$$\mathbf{P}_{k|k-1} = \mathbf{Q}_{k-1} + \sum_{i=0}^{M-1} W_{k-1}^i \left[\mathbf{f}_{k-1}(\chi_{k-1}^i) - \hat{\mathbf{x}}_{k|k-1}\right] \left[\mathbf{f}_{k-1}(\chi_{k-1}^i) - \hat{\mathbf{x}}_{k|k-1}\right]^T. \tag{62}$$

The predicted measurement is computed as:

$$\hat{\mathbf{z}}_{k|k-1} = \sum_{i=0}^{M-1} W_{k-1}^i \lambda_k(\chi_{k|k-1}^i). \tag{63}$$

Upon receiving the kth measurement z_k, the state and the state covariance are updated as follows:

$$\hat{\mathbf{x}}_{k|k} = \hat{\mathbf{x}}_{k|k-1} + \mathbf{K}_k(\mathbf{z}_k - \hat{\mathbf{z}}_{k|k-1}) \quad (64)$$

$$\mathbf{P}_{k|k} = \mathbf{P}_{k|k-1} - \mathbf{K}_k\mathbf{S}_k\mathbf{K}_k^T \quad (65)$$

where

$$\mathbf{K}_k = \mathbf{P}_{xz}\mathbf{S}_k^{-1} \quad (66)$$

is the filter gain and

$$\mathbf{S}_k = \mathbf{R}_k + \mathbf{P}_{zz} \quad (67)$$

is the innovation covariance. $\mathbf{P}_{xz}$ and $\mathbf{P}_{zz}$ are computed using:

$$\mathbf{P}_{xz} = \sum_{i=0}^{M-1} W_{k-1}^i(\chi_{k|k-1}^i - \hat{\mathbf{x}}_{k|k-1})(\lambda_k(\chi_{k|k-1}^i) - \hat{\mathbf{z}}_{k|k-1})^T \quad (68)$$

$$\mathbf{P}_{zz} = \sum_{i=0}^{M-1} W_{k-1}^i(\mathbf{h}_k(\chi_{k|k-1}^i) - \hat{\mathbf{z}}_{k|k-1})(\lambda_k(\chi_{k|k-1}^i) - \hat{\mathbf{z}}_{k|k-1})^T. \quad (69)$$

7.2 Simulation results

In order to compare the performance of proposed algorithms, we carried out 100 Monte Carlo runs using the scenario shown in Figure 10, where the crosses indicate the locations where the measurements are taken, and the star marks the location of the source. The source activity is set to $I = 10^6$, so that at the closest point of approach (205m away from the source), the SNR is 14dB. Other parameters used in simulations are: $\sigma_x = \sigma_y = 250$m, $\sigma_I = 10^5$, $N = 60$, $\lambda_b = 0.85$. The MLE, being a block algorithm, needs to be re-run every time a new measurement becomes available, in order to show the estimation error versus time. In addition, it is required to accumulate at least 33 measurements to run the MLE (otherwise it becomes unstable).

Figures 11 and 12 show the standard deviation of the estimation error for source position and activity, respectively. Analysis of the error performance results leads to the following observations. The EKF is diverging and is considered as unsuitable for this application. The UKF follows the trend of the CRB, but is somewhat worse than the bound. The MLE is indeed an asymptotically efficient (unbiased and minimum variance) estimator: its bias is approaching zero (not shown here) and its error standard deviation is approaching the CRB as more measurements become available for estimation. Finally we point out that the theoretical CRB is indeed a good predictor of the best achievable error performance.

8 Application to real radiological survey data

8.1 Holsworthy field trial data

To verify the theoretical analyses we applied them to a limited amount of real radiological survey data collected at Holsworthy Barracks, NSW in May 2005 during a field

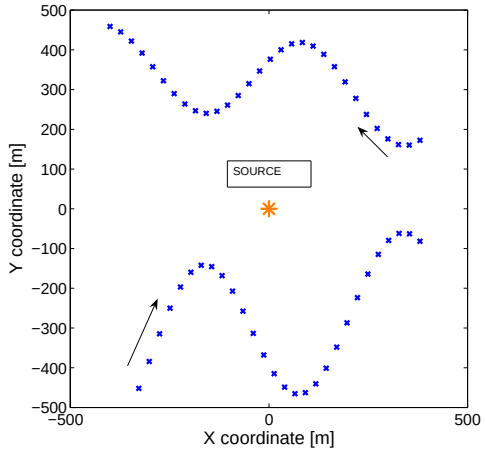

Figure 10: *The scenario used for simulation*

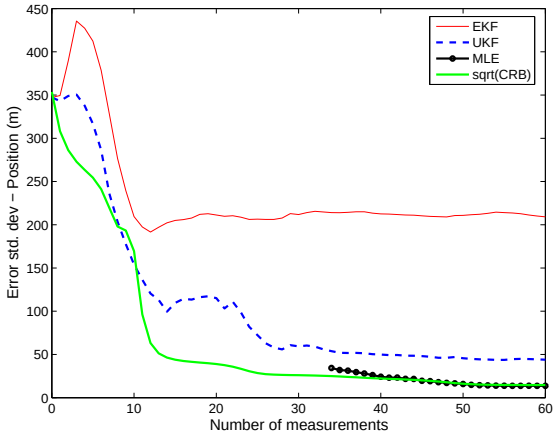

Figure 11: *The estimation error in position*

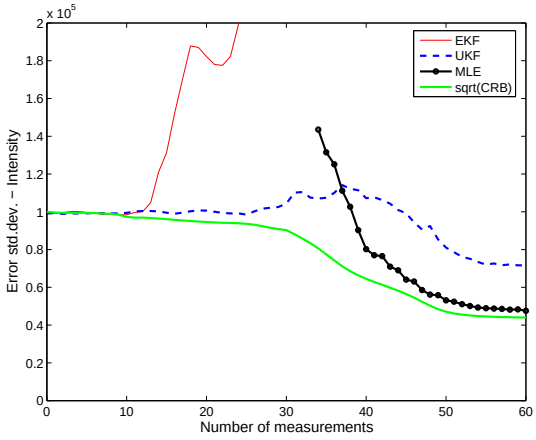

Figure 12: *The estimation error in source activity*

trial conducted to evaluate the LCAARS system.

Two point gamma radiation sources; a ^{60}Co source (source reference number 14) of approximately 0.3GBq activity emitting 1.17 and 1.33 MeV gamma radiation and a ^{137}Cs source (source reference number 23) of approximately 26.8 GBq emitting 0.662 MeV gamma radiation were used in the field trial. One set of dose rate data and one set of count rate data were collected with each one of the two radioactive sources emplaced. One set of background data was also collected with each detector in the absence of the sources. In addition to the dose rate or count rate data, GPS receiver readings of longitude and latitude of the detector position were also recorded. Because all estimation algorithms assume local Cartesian coordinates, longitude and latitude data were converted to Cartesian coordinates using the M_MAP mapping package. Unfortunately, due to some technical problems, the GPS coordinates of the two sources had not been recorded accurately and are known only approximately.

8.2 Deterministic solutions

The inverse distance square law-based analytical solution developed in Section 3 was applied to the real data from the Holsworthy trial. The four-point algorithm described therein requires as input the x and y coordinates at four arbitrary points and the radiation survey data measured at these four positions. For the purpose of illustration, the x and y coordinates and data at four points selected from the ^{137}Cs count rate data set are shown in Table 3.

Table 3: *An example set of four measurements from the ^{137}Cs count rate data used to demonstrate source estimation using the four point estimation algorithm*

x_1=1946.1	y_1=396.1	D_1=3950
x_2=2031.0	y_2=627.0	D_2=2820
x_3=1949.6	y_3=478.6	D_3=8860
x_4=1854.9	y_4=426.8	D_4=2150

Based on these four data points the algorithm estimated the source position as (2004.3, 491.2), which is in very good agreement with the true source position. In Figure 13 the blue circles show all positions at which measurements were collected, with the diameter of each circle indicating the relative magnitude of the corresponding measurement. The four red squares show the four measurements described in Table 3. The green dot and the black triangle denote the true source location and the estimated source location, respectively.

To test the reliability of the algorithm, a collection of 30 four-point groups were chosen from the ^{137}Cs count rate data and each group of four points was successively input to the algorithm. The estimates of source location obtained in these trials are shown in Figure 14. Except for one outlier (at (4205, 229)) out of the thirty estimates, the others are clustered closely around the true source position. It is remarkable that each estimate is based on only four measurements. Experimentation with the data shows that estimates may become unreliable if two or more of the four measurement points are too close to each other which is the case in the outlier in Figure 14.

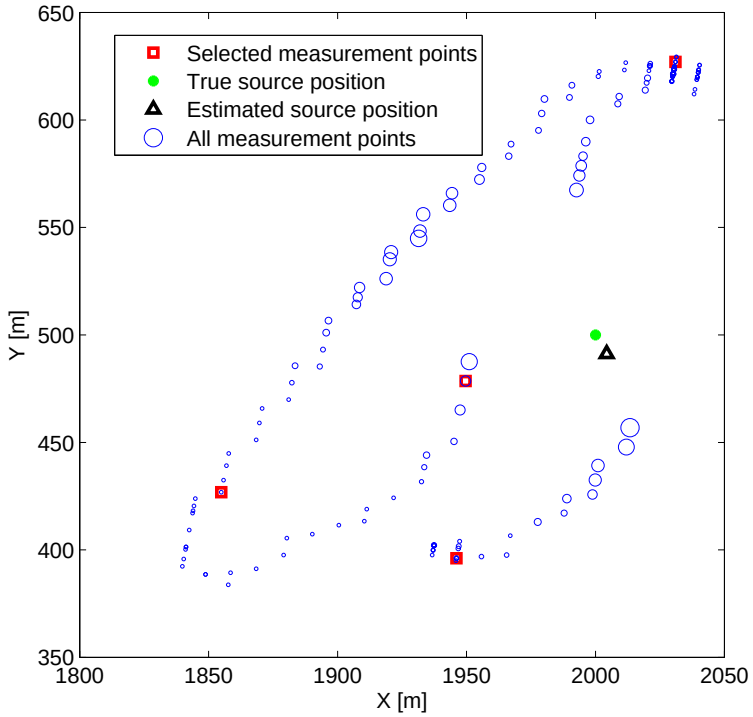

Figure 13: *An example application of the four point based deterministic source estimation algorithm.*

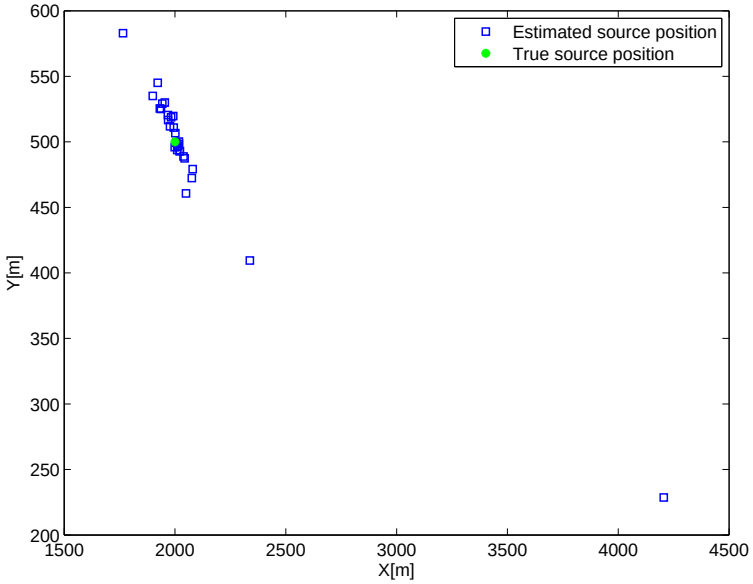

Figure 14: *The statistical spread of the estimated source location over a set of 30 four-point inputs.*

The estimation algorithm used here was developed assuming the measurements to be deterministic. Because the radioactive decay is a stochastic process rather than deterministic, the inverse square law is, actually, only applicable to the average values of measurements, rather than to the individual measurements. Therefore, we can expect the algorithm to produce more accurate and less variable source estimates if the mean values of measurements at the sampling points are used. We cannot investigate this hypothesis with the raw Holsworthy trial data, as only a single measurement had been collected at most sensor locations. During the field trial planned for October 2006, we intend to collect multiple measurements at each measurement location which would allow us to obtain the mean value at each position.

8.3 EKF, UKF and MLE

In subsection 4.1 it was shown that the normalised dose rate data were well modelled by a Poisson distribution. An appropriate model for measurement likelihood was proposed in Equation 24.

In order to apply the postulated model to real data collected in the field trial we require the mean value λ_b corresponding to the background data measured in situ. The normalised background dose rate data collected with the gamma probe in the field trial and a Poisson pdf fitted to this data are shown in Figure 15. From these data λ_b was estimated to be 0.8376, which is slightly larger than the value of 0.7946 estimated from laboratory data. The shielding provided by the concrete walls and the top floors of the building may be the reason for the lower background level inside the laboratory.

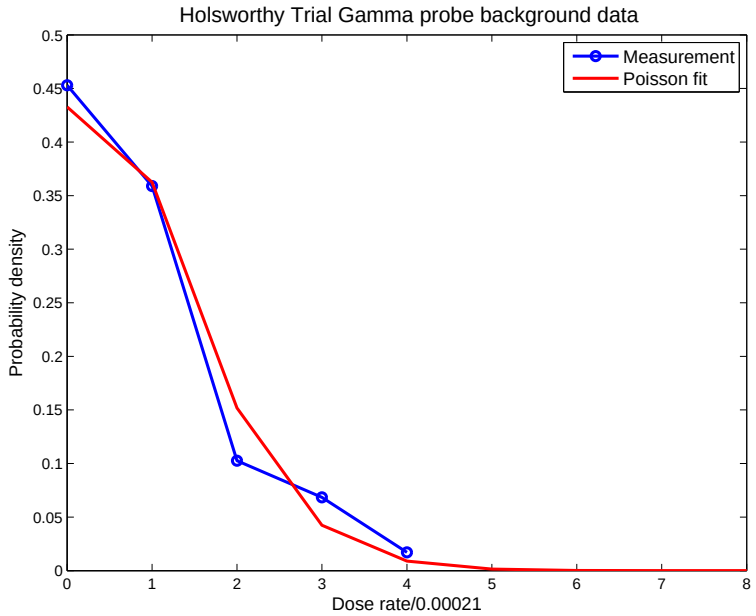

Figure 15: *The normalised histogram for background dose rate collected at Holsworthy army barracks and the Poisson distribution fitting*

Before we applied the estimation algorithms (MLE and UKF) we have discarded all

dose rate measurements with a normalised value lower than three. Both estimation algorithms were given the same prior information: the region where the source is located (500m × 500m) and the guessed value of source activity. For the MLE this prior information was used to initialise the *fminsearch* routine, while for the UKF this was the initial value of the state vector. In addition, the elements of $\mathbf{P}_0$ (required for UKF) were: $\sigma_x = \sigma_y = 125$m, $\sigma_I^2 = 10^7$. The results of our analysis are shown in Figure 16.

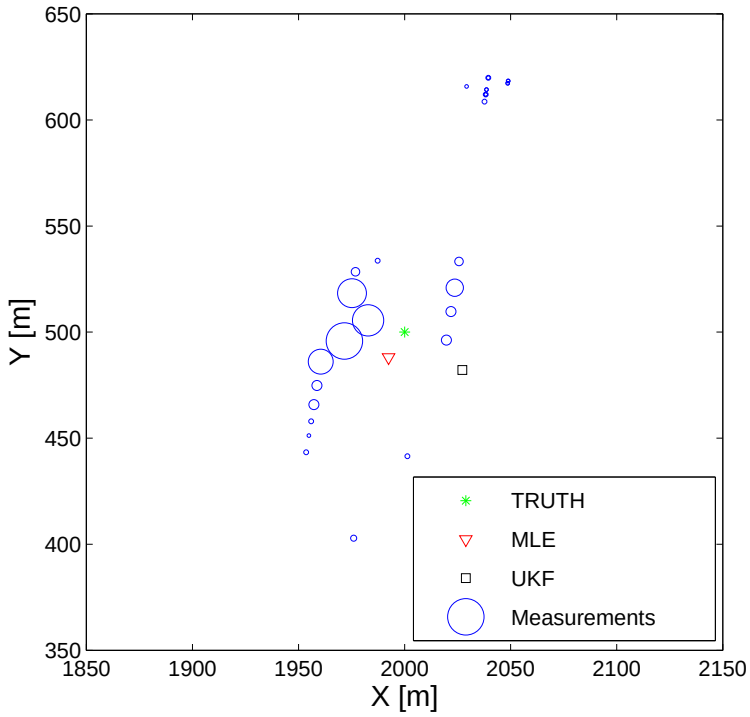

Figure 16: *Trial data analysis: Measurement locations/intensities (∘), true (∗) and estimated (□ and ▽) source locations*

Blue circles in Figure 16 show the locations and intensities of measured dose-rates. The centre of each circle indicated the location (x_k, y_k), while the radius of each circle corresponds to z_k. The approximate true location of the source is marked with a green $*$ symbol, the MLE and UKF estimates with a red triangle and a black square, respectively. Because the EKF diverged and failed to return a meaningful estimate these results are not shown here.

Figure 17 shows the actual measurements z_k (circles) versus $\lambda_k(\hat{\mathbf{x}})$ (crosses), where $\hat{\mathbf{x}}$ is the MLE estimate. The latter represents the mean of $p(z_k|\hat{\mathbf{x}})$, (Eqn 23). We observe a good agreement between the measurements and their prediction based on the MLE.

8.4 LS with reduced search dimension

We applied the LS algorithm with 2D search to the available radiation survey data. Figure 18 shows the sum squared error surface obtained for ^{137}Cs count rate data. The white circles show the locations where data were collected. The radius of each circle is used as a rough indicator of the relative magnitude of the measurements. Dark blue regions

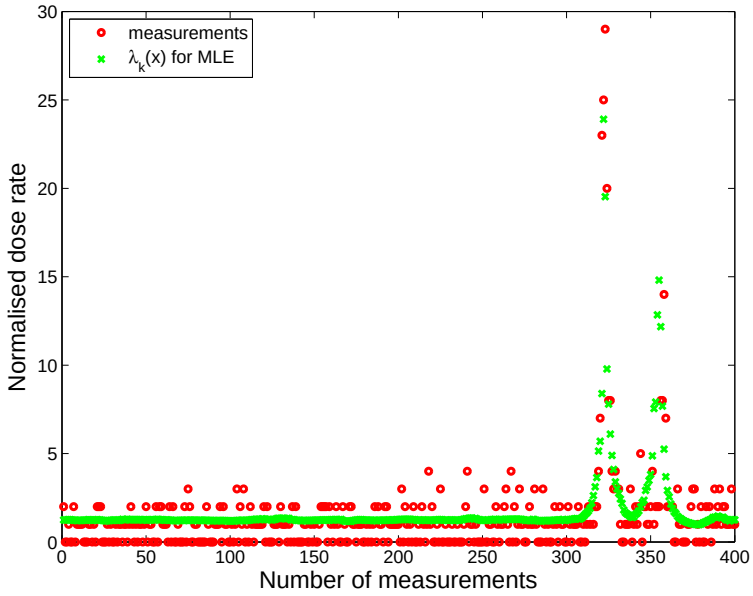

Figure 17: *Measured dose rates and* $\lambda_k(\mathbf{x})$ *corresponding to the MLE*

indicate source locations that lead to small values of sum squared error and, therefore, highly likely to be the true source position. Dark red regions correspond to positions that would lead to large values of sum squared error if the source were located there and, therefore, highly unlikely to be the true source position. The white square shows the location of the minimum error, which is chosen as the estimated source location. The green asterisk is the location where the true source was believed to be located. The estimated source position (2000, 510), is in good agreement with the true location, (2000, 500).

The distance from the estimated source position to each measurement point and the estimated source activity were used to predict the measurement values at these measurement locations. Figure 19 compares the measured data with the predictions.

The value of I was estimated to be 4.71×10^7. Using Equation (6) together with the energy response value of 12200 for the Micro-R probe for ^{137}Cs radiation the activity of the source is estimated to be:

$$\begin{aligned} M &= \left(4.71 \times 10^7 \times 6\right) / \left(12200 \times 0.662\right) \\ &= 35\ GBq \end{aligned}$$

which is of the same order as the true source activity of 26.8 GBq.

When the LS algorithm was applied to dose rate data collected with the ^{137}Cs source in place, it resulted in the error surface shown in Figure 20. Although the estimated source position (1957, 508) is about 43 m away from the true source position, the error surface correctly recognised the true source position also as highly likely, as indicated by the dark blue shade corresponding to very low error in this area. How the measurements predicted using the estimated source compare with the actual measurements is shown in Figure 21.

Figure 22 shows the error surface obtained for count rate data measured with the ^{60}Co source in place. In this case the source location estimated by the LS algorithm

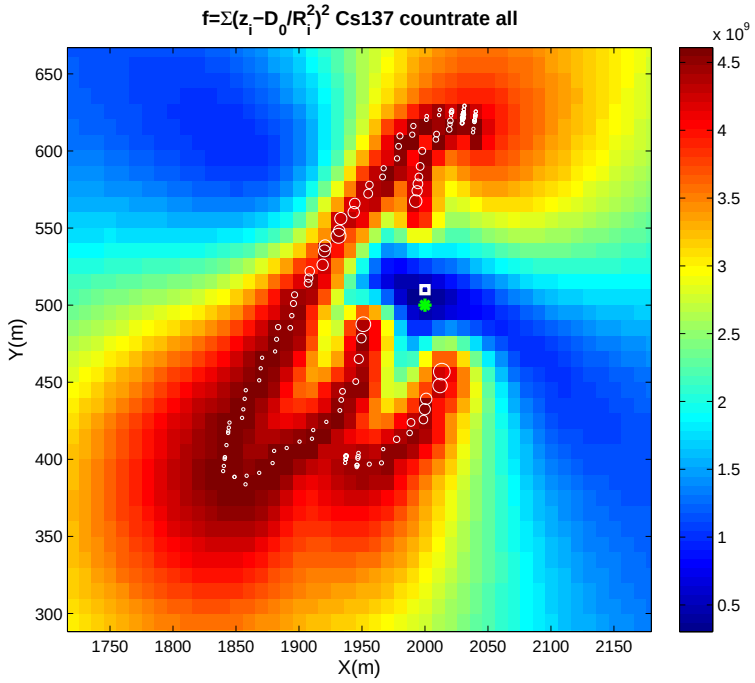

Figure 18: *The squared error surface obtained for* ^{137}*Cs count rate data. Measurement points (*$\circ$*) and the estimated (*$\square$*) and true (*$*$*) source positions are also shown.*

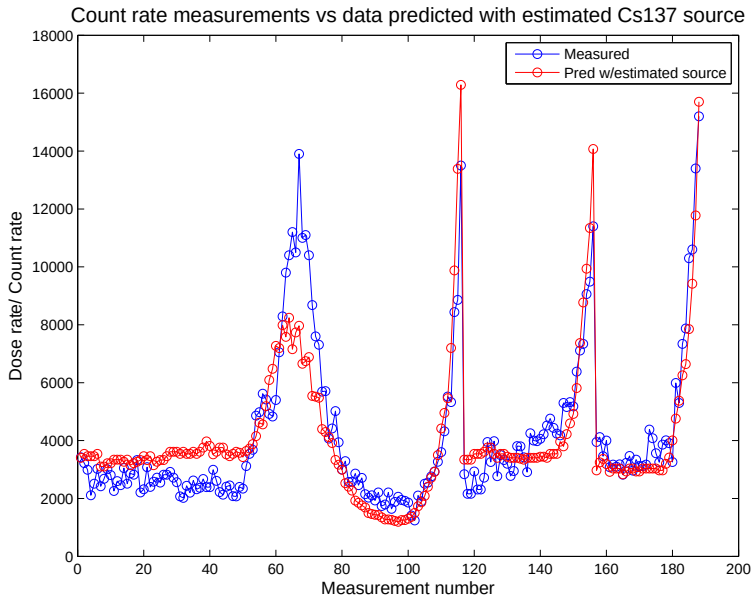

Figure 19: *Comparison of* ^{137}*Cs count rate measurements and prediction based on LS estimation*

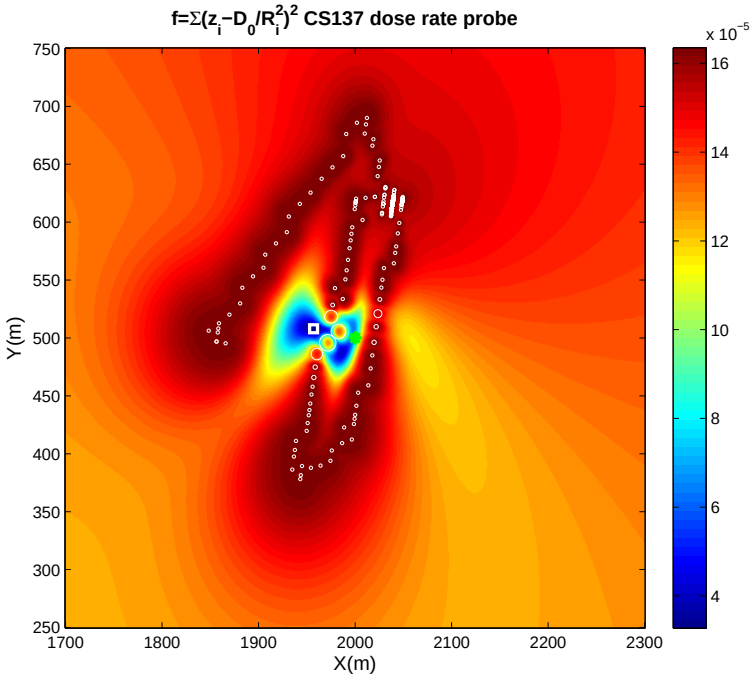

Figure 20: *The squared error surface obtained for* ^{137}Cs *dose rate data. Measurement points (*$\circ$*) and the estimated (*$\square$*) and true (*$*$*) source positions are also shown.*

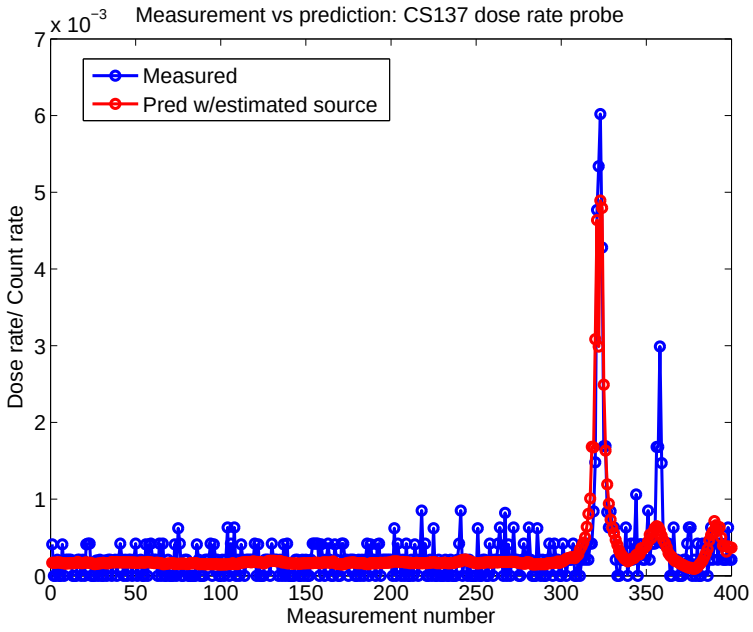

Figure 21: *Comparison of* ^{137}Cs *dose rate measurements and prediction based on LS estimation*

is different to the true source position. However, the dark blue region near the true source is an indication that this area is also highly likely to have the source. Because the measurements in this case are almost along a straight line, an image solution is, in fact, possible due to non-uniqueness. Therefore, if this algorithm is used in an operational situation, it may be prudent to search all areas that show low sum squared errors (dark blue areas in the plots). The measured and predicted data are compared in Figure 23. The error surface corresponding to dose rate data measured with the ^{60}Co source in place is shown in Figure 24. In this case the estimate is closer to the supposed true source position.

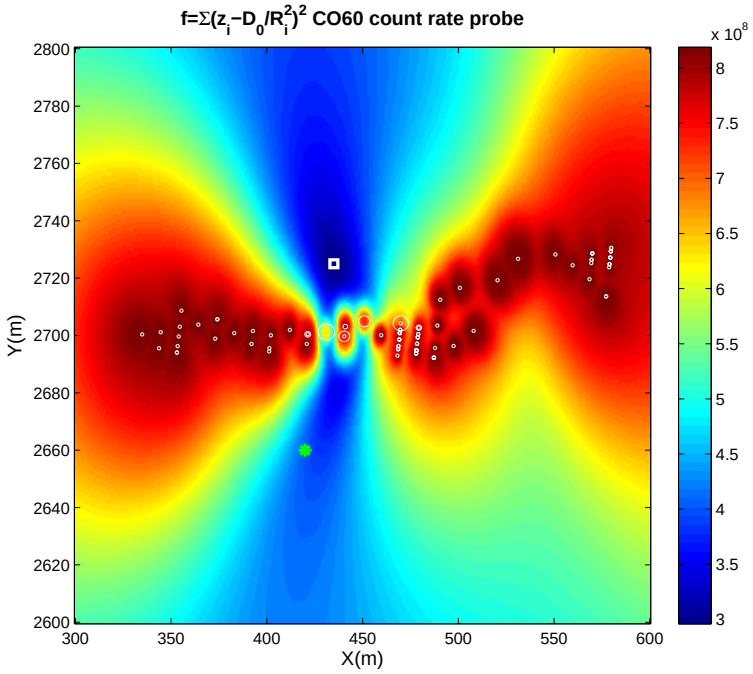

Figure 22: *The squared error surface obtained for ^{60}Co count rate data. Measurement points (∘) and the estimated (□) and true (∗) source positions are also shown.*

Figure 26 shows the error surface obtained for background count rate data measured in the absence of sources. The white square that denotes the estimated source location is at the top right corner of the picture, which is over 2 km away from the measurement location. The algorithm correctly recognised in this case that it would not be possible for a source to be present close to the measurement points.

These results indicate the LS algorithm to be a useful tool to locate an unknown single point gamma radiation source. It is particularly informative to look at the complete error surface and visualise all highly likely source locations than to simply rely on the single minimum returned by the algorithm. This fact was clearly demonstrated in some of the results presented above. While the results of applying the LS algorithm to Holsworthy trial data generally demonstrate its utility in locating point radiation sources, it is not possible to provide an exact measure of the accuracy of the estimates because the true source locations are known only approximately.

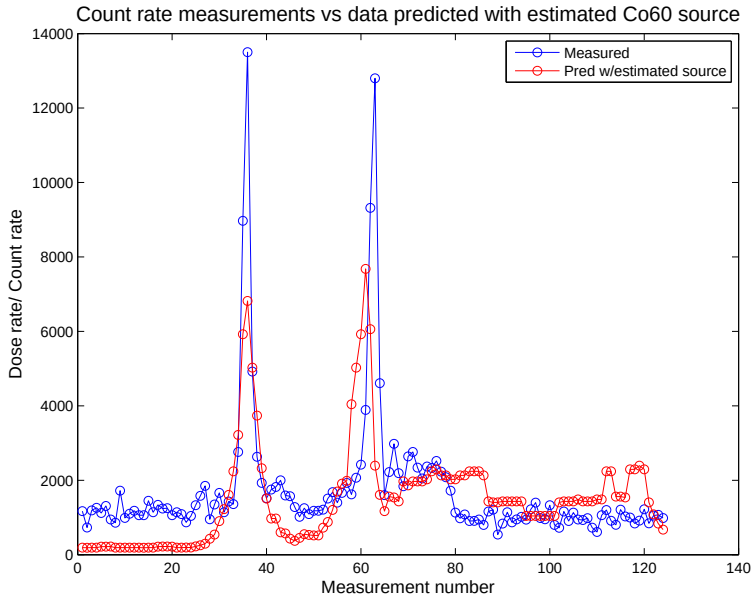

Figure 23: *Comparison of ^{60}Co count rate measurements and prediction based on LS estimation*

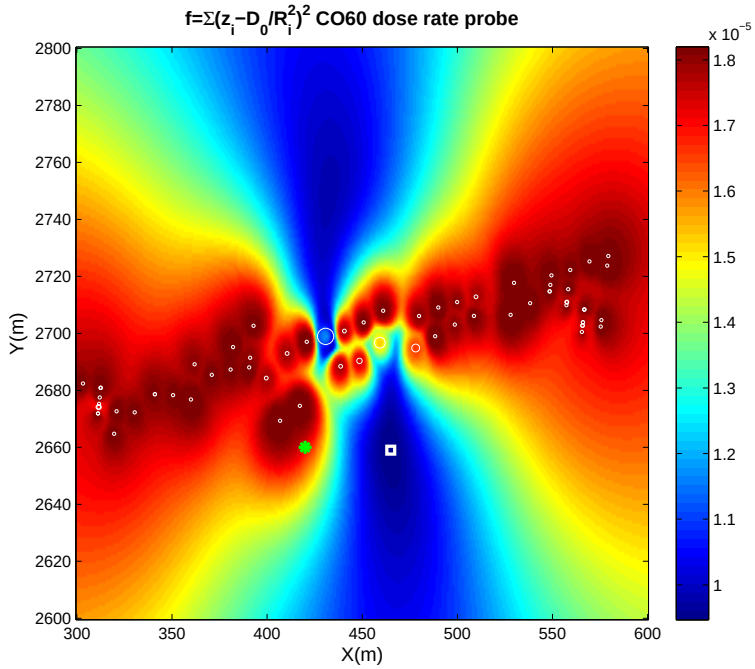

Figure 24: *The squared error surface obtained for ^{60}Co dose rate data. Measurement points ($\circ$) and the estimated ($\square$) and true ($*$) source positions are also shown.*

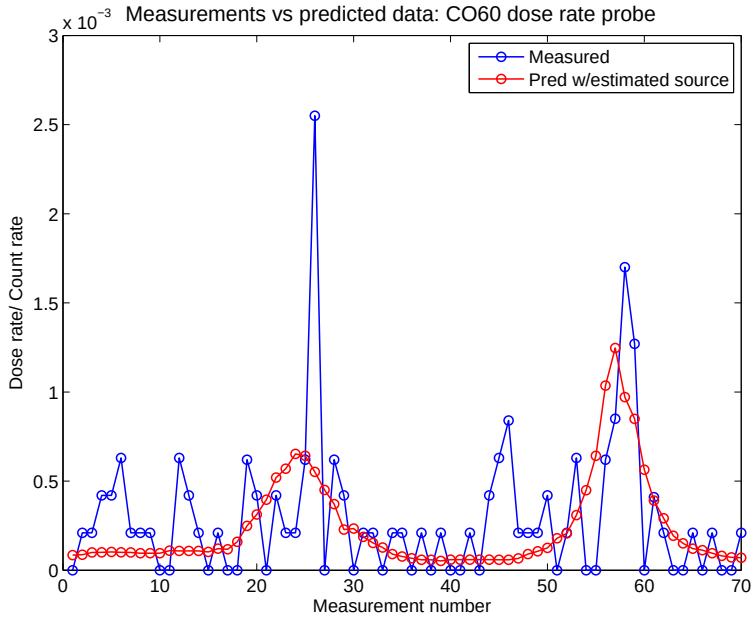

Figure 25: *Comparison of ^{60}Co dose rate measurements and prediction based on LS estimation*

8.5 The approximate recursive LS algorithm

An inexact LS algorithm to estimate the unknown radiation source based on radiation survey data in a recursive manner was described in Subsection 7.1.3. To check whether this inexact recursive algorithm could produce reasonable source estimates, it was applied to real data. Measured count rate/dose rate data were used to recursively update estimates of x_0, y_0 and I and the position estimation error was computed after each update. To compare the source estimates of the approximate recursive LS algorithm with those of the exact batch algorithm, the latter algorithm was also run repeatedly, varying the size of the batch from one to the full set of measurements. Plots comparing the progression of estimates for the approximate recursive algorithm and the exact batch algorithm for the case of ^{60}Co count rate data are shown in Figures 27(a)-(c). The corresponding progression of position errors for the two algorithms are compared in Figure 27(d). These plots indicate that the estimates of the recursive algorithm match those of the batch algorithm for these data. Similar agreement was obtained for the other data sets.

The estimates fluctuate rapidly until about the 70th measurement in the data shown, after which the estimates stabilise to the final value. From Figure 19 we see that this corresponds to a strong measurement peak. The early measurements are mostly low count rate data within the background level. Furthermore, because MLE is only asymptotically unbiased, estimates obtained with a small number of data points may be biased. The recursive algorithm seems to produce more fluctuations than the batch algorithm, initially, but after processing the first strong measurement peak it also converges rapidly to the correct estimates.

The recursive algorithm is quite attractive, as it can be used in real time. In a real operational scenario, obviously, the position error is not known. However, the plots of

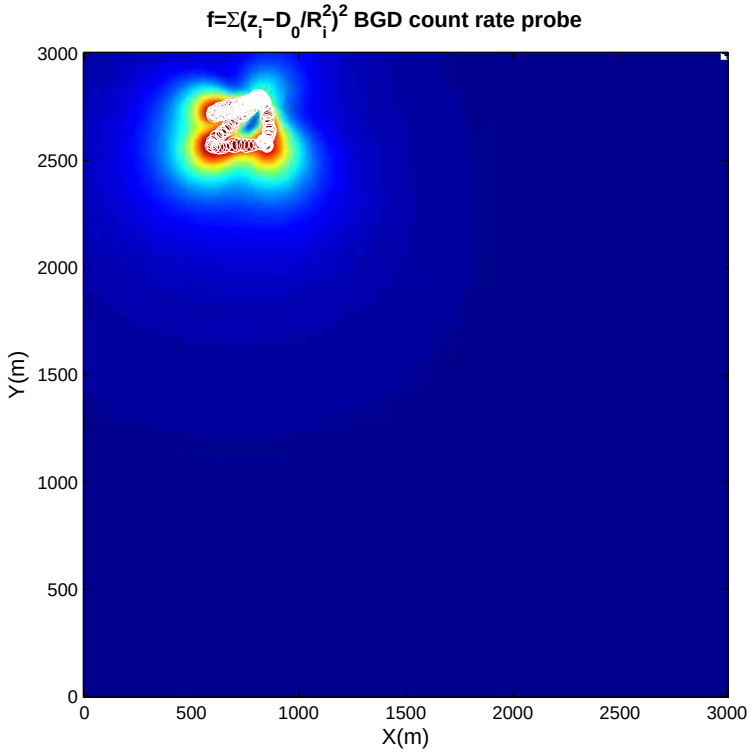

Figure 26: *The squared error surface obtained for background measurements. Measurement points are denoted by (∘) and the estimated source position by (□)*

estimates x_0, y_0 and I, similar to those in Figures 27(a)-(c) can be generated in real time. If the estimates stop fluctuating and stabilise to some values, this may be considered as an indication of convergence to a reliable source estimate. Once this is observed, it may be useful to move around this estimated source position and collect further measurements to refine the estimate. If the estimated source position were correct, moving towards this estimated location should produce measurements that are stronger on average. Of course, moving towards the estimated source should be done only as long as the measured count or dose rates do not exceed any predetermined maximum safe exposure levels.

Although this recursive algorithm performed well with the limited real data available from the Holsworthy trial, because it is an inexact algorithm, much more testing with real data should be carried out to validate it.

9 Conclusions

Several algorithms for estimating a single radiological point source were developed and studied using simulated and real radiological survey data.

A deterministic analytical solution based on the assumption of the inverse square law was able to provide rough source estimates using measurements collected at just four arbitrary points. Because the inverse square law is applicable to a radiological source only in an average sense, this algorithm can be expected to produce more stable and accurate

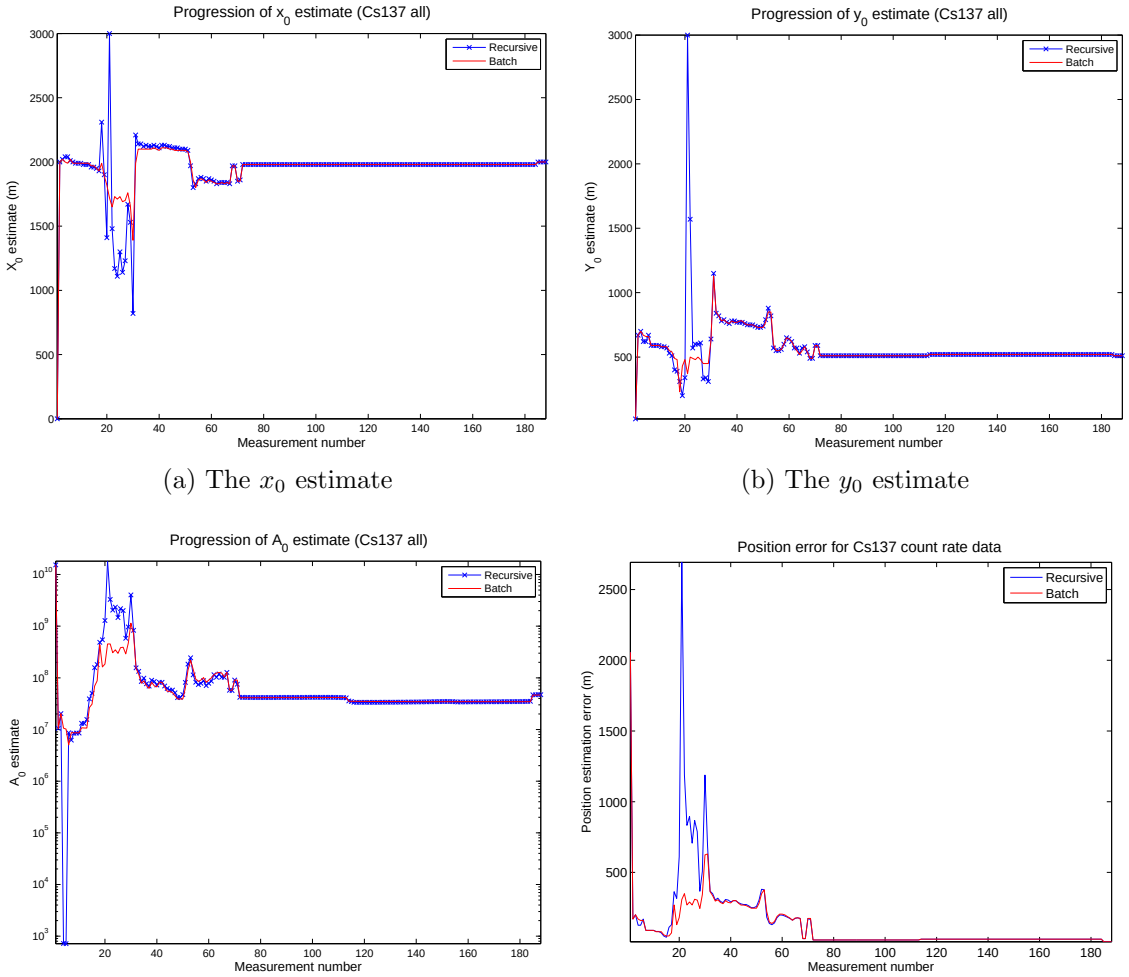

(a) The x_0 estimate

(b) The y_0 estimate

(c) The I estimate

(d) The position error

Figure 27: *The comparison of the batch LS algorithm with the approximate recursive LS algorithm for the case of* ^{137}Cs *count rate data*

estimates if averages of multiple sensor measurements collected at each position rather than individual readings are used as input to the algorithm.

The theoretical estimation lower bound known as the Cramer-Rao bound (CRB) was computed to visualise the observability of the source location and the activity. The maximum likelihood estimate (MLE) was obtained and, using simulation, it was shown to approach the theoretical bound predicted by the CRB analysis. When applied to real measurement data, the MLE was in good agreement with the known truth values. Although the MLE is an asymptotically optimal algorithm that approaches the theoretical bound when the number of measurements is large, being a batch algorithm, it is less attractive for operational use.

The unscented Kalman filter (UKF) and the extended Kalman filter (EKF) were also studied. While the estimation error of the UKF was worse than that of the MLE, it produced estimates that were reasonably close to the true source values. The EKF diverged and failed to produce acceptable estimates.

A least squares approach that uses an exhaustive search in a two dimension search space was investigated and shown to return good estimates. An inexact recursive version of this approach was developed. While this recursive algorithm produced reasonably accurate source estimates when applied to the limited set of real data available, its validity needs to be verified with more real data.

The radiological source localisation problem is a complex problem. The goal of research in this area is to be able to reliably estimate multiple possibly moving sources and, ultimately, track a cloud of radioactive particles. This report described our initial work towards understanding this difficult problem by first studying the relatively simple case of a single fixed radiological source.

We list below some possible research directions for future work.

1. Joint detection and localisation of multiple moving point sources

   Current work was based on prior knowledge that a single static point source is active in a region of interest. In reality this may not be realistic, and we may need to estimate both: (a) the number of point sources and (b) their location (with possibly other attributes). The sources may also be moving. Finally, it might be of interest to investigate the influence of the measurement location uncertainty (e.g. GPS accuracy is about 3m) on source localisation.

2. Localisation of point sources in a non-homogeneous radiation environment

   Current work assumes that the attenuation of the radiation is equal in all directions (e.g. open space homogeneous environment). In urban environments, with buildings and other obstacles, this will not be the case. For this situation it would be necessary to incorporate prior knowledge of obstacles (their placement and materials that determine their attenuation) into the localisation algorithms. A somewhat similar but different problem is to exploit prior knowledge of "forbidden" zones for the source location (e.g. secure areas).

3. Diffusive sources

Current work focused on point sources only. In some situations it may be more realistic to use a model of spatial and temporal concentration distribution of the dispersed substance (chemical, radiological) from a diffusion source (e.g. a particle cloud resulting from a dirty bomb explosion). The goal in this case would be to track the centroid and the spread of the cloud over time. In the case of a chemical spill, it may be required to localise the source of diffusion.

4. Investigation of Wireless sensor network technology for CBRN data fusion

   Recent advances in wireless sensor networks (WSNs) technology have enabled deployment of a large number of tiny smart sensor nodes for monitoring space and objects. The unique aspect of WSNs is that they integrate wireless communication, sensing and computation. It would be of interest to investigate the use of tiny CBRN sensors (for example carried by soldiers) and their fusion for monitoring and localisation of CBRN hazards in a region of interest. Various aspects of this emerging technology would need to be examined, such as the fusion architecture (centralised vs distributed), network bandwidth and latency constraints, protocols, etc.

5. Optimisation of observer(s) trajectory

   The problem is to guide the motion of (possibly multiple) observers in order to localise the source in the quickest possible manner [17]. For example, suppose that we know that the source is inside a certain region, and we perform on-line (recursive) source position estimation. Then intuitively it seems that the observer(s) should move towards the currently estimated source location, in order to get more informative measurements and localise the source quicker. The observer motion should be constrained by the safety of observer(s). Alternatively, in the WSN context, we may want to select a subset of sensors to transmit the measurements, in order to save the batteries (transmissions require energy and should be minimised in order to extend the lifespan of a network).

References

1. R. Gailis, "CBR data fusion and situational awareness," Tech. Rep. DSTO-CR-2005-0167, DSTO, 2005.
2. Glenn F Knoll, *Radiation detection and measurement*, John Wiley, 2nd edition, 1989.
3. A. Martin and S. A. Harbison, *An introduction to radiation protection*, Chapman & Hall, 1987.
4. *AN/PDR-77 Users Guide (Including Micro-R probe and Pancake beta probe).*
5. Y. Bar-Shalom, X. R. Li, and T. Kirubarajan, *Estimation with Applications to Tracking and Navigation*, John Wiley & Sons, 2001.
6. P. Robins and P. Thomas, "Non-linear Bayesian CBRN source term estimation," in *Proc. Intern. Conf. Information Fusion*, Philadelphia, PA, USA, July 2005.
7. J. H. Taylor, "The Cramer-Rao estimation error lower bound computation for deterministic nonlinear systems," *IEEE Trans. Automatic Control*, vol. 24, no. 2, pp. 343–344, April 1979.
8. B. Ristic, S. Arulampalam, and N. Gordon, *Beyond the Kalman filter: Particle filters for tracking applications*, Artech House, 2004.
9. A. Gunatilaka, B. Ristic, and R. Gailis, "On localisation of a radiological point source," in *Proc. Information, Decision and Control conference*, Adelaide, Australia, Feb. 2007.
10. H. L. VanTrees, *Detection, Estimation and Modulation Theory (Part I)*, John Wiley & Sons, 1968.
11. W. H. Press, B. P. Flannery, S. A. Teukolsky, and W. T. Vetterling, *Numerical recipes in C*, Cambridge Univ. Press, 2nd edition, 1992.
12. I. Takumi, M Nagai, S. Kato, M. Hata, and H. Yasukawa, "Estimation of EM source location from 223 Hz EM field power data at multiple spots," in *IEEE Intern. Geoscience and Remote Sensing Symposium (IGARSS'01)*, July 2001, vol. 7, pp. 3191 – 3193.
13. Yaakov Engel, Shie Mannor, and Ron Meir, "The kernel recursive least-squares algorithm," *IEEE Transactions on Signal Processing*, vol. 52, no. 8, pp. 2275–2285, 2004.
14. G Haupt, N Kasdin, G Keiser, and B Parkinson, "An optimal recursive iterative algorithm for discrete nonlinear least-squares estimation," in *AIAA Guidance, Navigation and Control Conference*, Baltimore, MD, 1995, AIAA-95-3218, pp. 404–417.
15. James W Howse, Lawrence O Ticknor, and Kenneth R Muske, "Least squares estimation techniques for position tracking of radioactive sources," *Automatica*, vol. 37, pp. 1727–1737, 2001.
16. S. Julier, J. Uhlmann, and H.F.Durrant-White, "A new method for nonlinear transformation of means and covariances in filters and estimators," *IEEE Trans. Automatic Control*, vol. 45, no. 3, pp. 477–482, March 2000.
17. Alexei V. Klimenko, William C Priedhorsky, Nicolas W Hengartner, and Konstantin N Borozdin, "Efficient strategies for low-statistics searches," *IEEE Transactions on Nuclear Science*, vol. 53, no. 3, pp. 1435–1442, 2006.

Appendix A Derivation of the analytical solution

Let us consider measurements $\{z_k, k = 1, 2, 3, 4\}$ collected at four arbitrary points (x_k, y_k). If we disregard noise and background radiation, these measurements can be expressed as:

$$z_k(\mathbf{x}) = I/r_k^2, \qquad k = 1, 2, 3, 4 \tag{A1}$$

where

$$r_k = \sqrt{(x_k - x_0)^2 + (y_k - y_0)^2} \tag{A2}$$

is the distance from the source (x_0, y_0) to the kth measurement point (x_k, y_k).

These four equations can be rewritten as follows:

$$\begin{aligned}
(x_1 - x_0)^2 + (y_1 - y_0)^2 &= I/z_1 && \text{(A3)}\\
(x_2 - x_0)^2 + (y_2 - y_0)^2 &= I/z_2 && \text{(A4)}\\
(x_3 - x_0)^2 + (y_3 - y_0)^2 &= I/z_3 && \text{(A5)}\\
(x_4 - x_0)^2 + (y_4 - y_0)^2 &= I/z_4. && \text{(A6)}
\end{aligned}$$

By subtracting Eqn (A4) from Eqn(A3) we get:

$$(x_1^2 - x_2^2) - 2(x_1 - x_2)x_0 + (y_1^2 - y_2^2) - 2(y_1 - y_2)y_0 = \frac{I}{z_1} - \frac{I}{z_2}. \tag{A7}$$

Similarly, by subtracting Eqn (A5) and Eqn (A6), respectively, from Eqn (A3) we obtain:

$$(x_1^2 - x_3^2) - 2(x_1 - x_3)x_0 + (y_1^2 - y_3^2) - 2(y_1 - y_3)y_0 = \frac{I}{z_1} - \frac{I}{z_3}. \tag{A8}$$

and

$$(x_1^2 - x_4^2) - 2(x_1 - x_4)x_0 + (y_1^2 - y_4^2) - 2(y_1 - y_4)y_0 = \frac{I}{z_1} - \frac{I}{z_4}. \tag{A9}$$

By dividing Eqn (A7) by Eqn (A8), we get:

$$\frac{(x_1^2 - x_2^2) - 2(x_1 - x_2)x_0 + (y_1^2 - y_2^2) - 2(y_1 - y_2)y_0}{(x_1^2 - x_3^2) - 2(x_1 - x_3)x_0 + (y_1^2 - y_3^2) - 2(y_1 - y_3)y_0} = \frac{\frac{I}{z_1} - \frac{I}{z_2}}{\frac{I}{z_1} - \frac{I}{z_3}}. \tag{A10}$$

Similarly, the division of Eqn (A7) by Eqn (A9) gives:

$$\frac{(x_1^2 - x_2^2) - 2(x_1 - x_2)x_0 + (y_1^2 - y_2^2) - 2(y_1 - y_2)y_0}{(x_1^2 - x_4^2) - 2(x_1 - x_4)x_0 + (y_1^2 - y_4^2) - 2(y_1 - y_4)y_0} = \frac{\frac{I}{z_1} - \frac{I}{z_2}}{\frac{I}{z_1} - \frac{I}{z_4}}. \tag{A11}$$

Next, we define the following variables:

$$\begin{aligned}
K_1 &= \frac{\left(\frac{1}{z_1} - \frac{1}{z_2}\right)}{\left(\frac{1}{z_1} - \frac{1}{z_3}\right)}\\
K_2 &= \frac{\left(\frac{1}{z_1} - \frac{1}{z_2}\right)}{\left(\frac{1}{z_1} - \frac{1}{z_4}\right)}\\
L_1 &= (x_1^2 - x_2^2) + (y_1^2 - y_2^2)\\
L_2 &= (x_1^2 - x_3^2) + (y_1^2 - y_3^2)\\
L_3 &= (x_1^2 - x_4^2) + (y_1^2 - y_4^2).
\end{aligned}$$

By plugging in these factors in Eqn (A10) and Eqn (A11) and rearranging, we obtain:

$$a_1 x_0 + b_1 y_0 + c_1 = 0 \tag{A12}$$

$$a2x_0 + b_2 y_0 + c_2 = 0 \tag{A13}$$

where

$$\begin{aligned} a_1 &= 2K_1(x_1 - x_3) - 2(x_1 - x_2) \\ b_1 &= 2K_1(y_1 - y_3) - 2(y_1 - y_2) \\ c_1 &= L_1 - K_1 L_2 \\ a_2 &= 2K_2(x_1 - x_4) - 2(x_1 - x_2) \\ b_2 &= 2K_2(y_1 - y_4) - 2(y_1 - y_2) \\ c_2 &= L_1 - K_2 L_3. \end{aligned}$$

By solving Eqn (A12) and Eqn (A13) simultaneously, we find x_0 and y_0 as:

$$x_0 = \frac{b_1 c_2 - c_1 b_2}{a_1 b_2 - b_1 a_2} \tag{A14}$$

$$y_0 = \frac{a_1 c_2 - c_1 a_2}{b_1 a_2 - a_1 b_2}. \tag{A15}$$

By inserting the values of x_0 and y_0 in Eqn (A3), we compute the source activity I as:

$$I = z_1 \left[(x_1 - x_0)^2 + (y_1 - y_0)^2 \right]. \tag{A16}$$

Page classification:

DEFENCE SCIENCE AND TECHNOLOGY ORGANISATION DOCUMENT CONTROL DATA				1. CAVEAT/PRIVACY MARKING
2. TITLE Radiological Source Localisation			3. SECURITY CLASSIFICATION Document (U) Title (U) Abstract (U)	
4. AUTHORS Ajith Gunatilaka, Branko Ristic, and Ralph Gailis			5. CORPORATE AUTHOR Defence Science and Technology Organisation 506 Lorimer St, Fishermans Bend, Victoria 3207, Australia	
6a. DSTO NUMBER DSTO–TR–1988	6b. AR NUMBER 013-892		6c. TYPE OF REPORT Technical Report	7. DOCUMENT DATE July, 2007
8. FILE NUMBER 2007/1026872/1	9. TASK NUMBER DST 05/161	10. SPONSOR CCT Sponsor	11. No OF PAGES 38	12. No OF REFS 17
13. URL OF ELECTRONIC VERSION http://www.dsto.defence.gov.au/corporate/reports/DSTO–TR–1988.pdf			14. RELEASE AUTHORITY Chief, Human Protection and Performance Division	
15. SECONDARY RELEASE STATEMENT OF THIS DOCUMENT *Approved For Public Release* OVERSEAS ENQUIRIES OUTSIDE STATED LIMITATIONS SHOULD BE REFERRED THROUGH DOCUMENT EXCHANGE, PO BOX 1500, EDINBURGH, SOUTH AUSTRALIA 5111				
16. DELIBERATE ANNOUNCEMENT No Limitations				
17. CITATION IN OTHER DOCUMENTS No Limitations				
18. DSTO RESEARCH LIBRARY THESAURUS Hazard analysis				
19. ABSTRACT The problem of localising a point source of gamma radiation is considered. A simplified analytical approach based on the inverse distance square law as well as several probabilistic approaches are described. The problem is studied using the Cramer-Rao bound (CRB) analysis, which quantifies the accuracy with which it is possible to localise the source and estimate its activity. Simulated and real radiological survey data are used to investigate the performance of the algorithms.				

Page classification: